Title
Bacteria-Inorganic Hybrids for Bio-Energy Harvesting

Author
Cao, Bocheng

Publication Date
2021

Peer reviewed|Thesis/dissertation

UNIVERSITY OF CALIFORNIA

Los Angeles

Bacteria-Inorganic Hybrids for Bio-Energy Harvesting

A dissertation submitted in partial satisfaction of the

requirements for the degree

Doctor of Philosophy in Department of Chemistry and Biochemistry

by

Bocheng Cao

2021

ABSTRACT OF THE DISSERTATION

Bacteria-Inorganic Hybrids for Bio-Energy Harvesting

by

Bocheng Cao
Doctor of Philosophy in Department of Chemistry and Biochemistry
University of California, Los Angeles, 2021
Professor Xiangfeng Duan, Chair

Exoelectrogenic bacteria can transfer the electrons out of the cell body through the extracellular electron transfer (EET) process after consuming various organic matters, which attracts increasing attentions in both academia and industrial communities. In this dissertation, I will focus on a typical exoelectrogenic bacterium *Shewanella* and its cooperating with inorganic materials such as nano-devices and nanoparticles. In the *Shewanella*-nano-devices hybrids, the current output features and cell density can be both *in-situ* monitored and studied. Take a further step, by anchoring the metal nanoparticles into the *Shewanella* membrane structures and bulk biofilms, we can greatly boost the EET process and achieve record high power output.

In the first project, we developed and applied an on-chip approach to study the EET, metabolic activity status and behaviors of microbes for maximal current production with real time *in-situ* microscope observation. The dissimilatory extroelectrogenic bacteria *Shewanella oneidensis* MR-1 wild type (WT) and its mutant cells (Δbfe and ΔmtrC/ΔomcA) were used as the model organisms to understand extroelectrogenic biofilm growth, metabolism rate, and current

production. Our goal is to specify the various mechanisms of EET process in *Shewanella oneidensis* MR-1 and its mutant cells under different conditions.

Furthermore, based on the insight developed from the on-chip platform, we further develop a rational strategy to boost the transmembrane and extracellular electron transfer processes by loading *Shewanella* biofilms on reduced graphene oxide/silver nanoparticles (rGO/Ag) scaffolds. Our systematic studies show that the rGO/Ag can release positively charged silver ions, which facilitate *Shewanella* attachment to rGO/Ag scaffold to form dense biofilms, while at the same time produce transmembrane and outer-membrane Ag nanoparticles to form the *Shewanella*-Ag hybrids, with greatly enhanced transmembrane and extracellular electron transfer efficiency to improve the bacteria turn-over frequency (TOFs) and boost the overall *Shewanella* based microbial fuel cells (MFCs) performance. The resulting MFCs with the rGO/Ag anode can output a current density of 38.5 A/m^2, a power density of 6.63 W/m^2 and a Coulombic efficiency of 81%, greatly outperforming the best *Shewanella* MFCs reported to date.

In the third project, we further show that rGO/Cu scaffolds can exert a similar enhancement effect to produce high performance in the MFC tests, demonstrating universal applicability of our strategy for enhancing the MFC performance.

The dissertation of Bocheng Cao is approved.

William G. Gelbart

Thomas G. Mason

Richard B. Kaner

Xiangfeng Duan, Committee Chair

University of California, Los Angeles

2021

To my parents, my families and my love, who made me tough and full of hopes

Table of contents

List of Figures

List of Tables

ACKNOWLEDGMENTS

The past five years in the Department of Chemistry and Biochemistry, University of California, Los Angeles was really a fantastic journey. I would like to take this chance to express my sincere appreciation to the people who helped me during the impressive five years.

First and foremost, I would like to greatly thank my advisor, Prof. Xiangfeng Duan, for his invaluable guidance on my research. Throughout my long journey as a graduate student, I have always been impressed by his profound knowledge and keen insight to find interesting scientific problems, and also his incomparable passion and faith in science. “There is no magic in the research. The more you see and do, the more freedom you’ll get in the mind”, the words he told me has been encouraging and impressing me for all the time. Also I would like to greatly thank my co-advisor, Prof. Yu Huang, for her great support and patience. Her constant enthusiasm for keeping generating fantastic ideas and methods helps me solve numerous unexpected problems in my research.

I would like to thank the members on my thesis committee. Prof. Thomas G. Mason, thank you for your encouragement in the thermal and statistic course when I was so depressed. Prof. Richard B. Kaner, thank you for your fantastic journey you brough to me in the solid state and chemistry course. Prof. William M. Gelbart, thank you for your warm welcome when I came to the chemistry department in the first day. Besides, I would like to thank you all for reading my thesis and providing valuable feedback, as well as be greatly helpful on my oral qualification exam, 4th year meeting and the career plan.

I was also having a great time working with our outstanding group members. In particular, Dr. Hui-ying Shiu taught me plenty of knowledge of bacteria and fabrication. Dr. Mengning Ding

impressed me with his enthusiasm in research. Dr. Zipeng Zhao is always kind and helpful to every question I had raised, for which I have been always grateful. I admire Dr. Hao Jing for his patience when I first start my research life. Dr. Yiliu Wang, who is always a tough guy and being a great working-out partner, helped me a lot in adapting to the new group. Dr. Enbo Zhu and Dr. Ziying Feng also gave me lots of valuable suggestions in career plans. Dr. Mufan Li, Dr. Xiang Xu, Dr. Huilong Fei, Dr. Chengzhang Wan, Guangyan Zhong, and Wang Xue, Jin Huang, we were having a wonderful time in a basketball team. Dr. Dan Baumann, Frank Song, Dan Zhu and Xiaoyang Fu, I'll always remember the great time we had in the same room.

Last but not least, I am enormously grateful to my parents, my families and my love Yutong Wu, without whom I cannot make it.

VITA

2016 B.S. (Chemistry) and B.S. (Business management), Jilin University.

2018 M.S. (Material Chemistry), UCLA, Los Angeles, California.

2021 Dissertation Award for Excellence in Inorganic Chemistry

Chapter 1. Introduction

1.1 Exoelectrogenic bacteria

Bacteria is one of the largest species in the world (**Fig. 1.1**) with the estimated number of 5×10^{30}, which is far larger than the total cells number contained in all animals and human[1]. Some of bacteria can cause severe health problems, which are still regarded as medical challenges need to be solved. On the other hand, for some other bacteria like probiotics, our body and organs can perform and operate under a better condition with their existence and help[2]. For example, the *Saccharomyces* in our stomach and intestine can help us to digest food better and faster. In industries, they can also help produce certain breads and wines in numerous factories[3]. As new species of bacteria are discovered continuously, some of the bacteria can even help solve the energy crisis problem due to the special features owing to their distinguished structures.

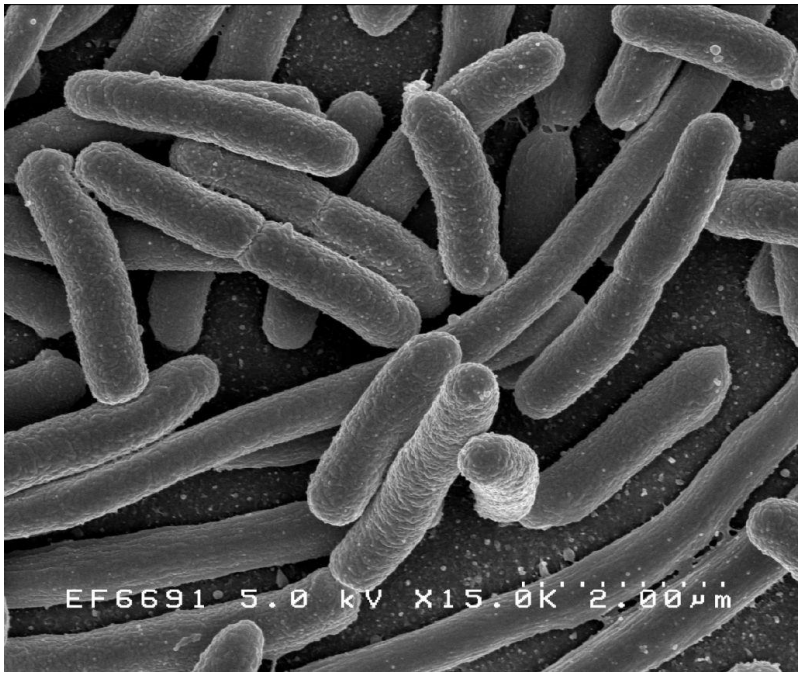

Fig. 1.1. The typical *E. coli* bacteria shape and structure. According to various species of bacteria, the shape and specific structure may be different. *Adapted from https://en.wikipedia.org/ /wiki/Bacteria/media.*

For a most common bacterium, the energy needed for metabolism is mainly from the organic matter consuming process[4]. In general, this process can be summarized as the organic matter being consumed inside the bacterium body with the help of certain enzymes. The resulting products will further combine with oxygen or other electron acceptors to produce the water, carbon dioxide and release chemical energy in the form of ATPs. Meanwhile, the electrons produced when consuming the organic matter can be well depleted by the oxygen and other electron acceptors. Nevertheless, some bacteria, due to the special protein channels on the membrane structure, can surprisingly transfer some of the electrons to the outside bacterium body when there is no enough of electron acceptors. For these kinds of bacteria, they have a special name called exoelectrogenic bacteria[5].

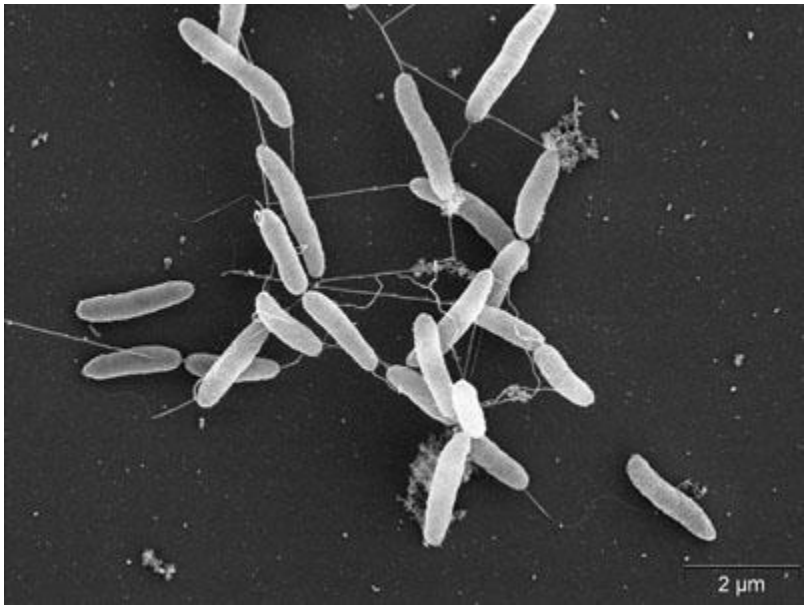

Fig. 1.2. *Shewanella* bacteria (bar like) on the flat electrode. *Adapted from https://genome.jgi.doe.gov/portal/she_m/she_m.home.html*

Interestingly, the word ‘exoelectrogenic’ is from a combined verbal result. The ‘exo’ is the brief form of the extracellular, during which process the electrons are transferred from inner cell

to the outer cell. The 'electro' well describes that it is the electron being transferred during this process and this will make such bacterium own some electrical features. The exoelectrogenic process is realized due to the special protein channels lying on the bacteria inner and outer-membrane. The first found and purified exoelectrogenic bacteria is *Shewanella* **(Fig. 1.2)**.

Shewanella is firstly discovered in the soil with rich iron oxide sediment and also, they are found on the surface of rusted iron. After conducting the gene and proteomics analysis, the scientist found several kinds of cytochromes on the inner and outer-membrane to help the electron transfer. This is the main reason why *Shewanella* tends to find and attach to the metal oxide for better transfer of the electron[6].

Within the *Shewanella*, the metabolic tricarboxylic acid cycles (TCA) in the bacteria cytoplasm will produce electrons in the form of electron carriers (nicotinamide adenine dinucleotide, NADH)[7], which transfers the electrons to quinones near the inner membranes to produce quinols[8,9]. The electrons stored in quinols can then go across the periplasm between the inner membrane and the outer membrane through the multistep hopping between the cytochrome redox centers (**Fig. 1.3**). On the outer membrane, the electrons are transferred to the electrode surface through a series of direct or indirect extracellular electron transfer process[10,11,12]. So that in the process, the bacteria are acting like a cell-level catalyst that help release the chemical energy restored in the organic matter in the form of electricity.

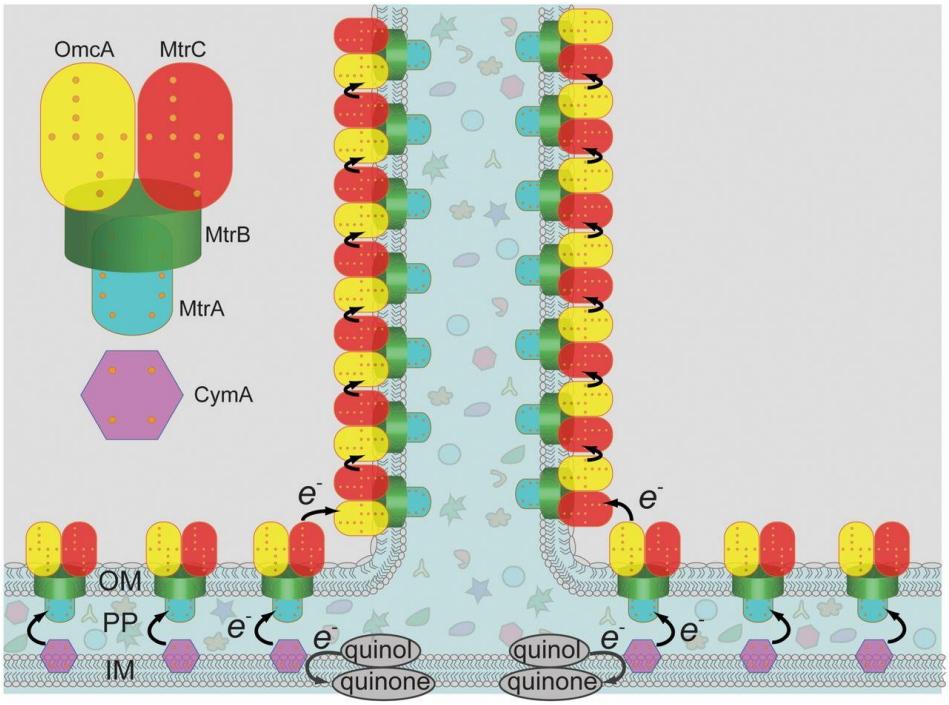

Fig. 1.3. The membrane structure of *Shewanella*. The CymA and MtrABC are the cytochrome protein that can help transfer the electron between redox center. *Adapted from Ref. 10*

1.2 Microbial Fuel Cell

Fuel cell is the device that convert the chemical energy restored in the fuel molecules to the electric energy[13]. In a typical fuel cell, the fuel is usually oxidized at the anode, which will produce the electron and other byproducts like protons and carbon dioxide (CO_2). The electrons will go through the outer fuel cell circuit and finally reach the cathode, where they will combine with the oxygen and produce the water during the oxygen reduction reaction (**Fig. 1.4**). The fuel molecules include but not limit to methanol, ethanol and hydrogen. In the past decades, with the help of new generation of noble metal based catalyst like Pt/Ni nanoparticles, the fuel cell can be even put into the practical use with extraordinary performance[14]. The exoelectrogenic bacteria, which can also convert the fuel chemical energy to the electricity, can also act like the bio-catalyst in the fuel cell.

When combining the bacteria catalyst into the fuel cell, we can construct the microbial fuel cell (MFC).

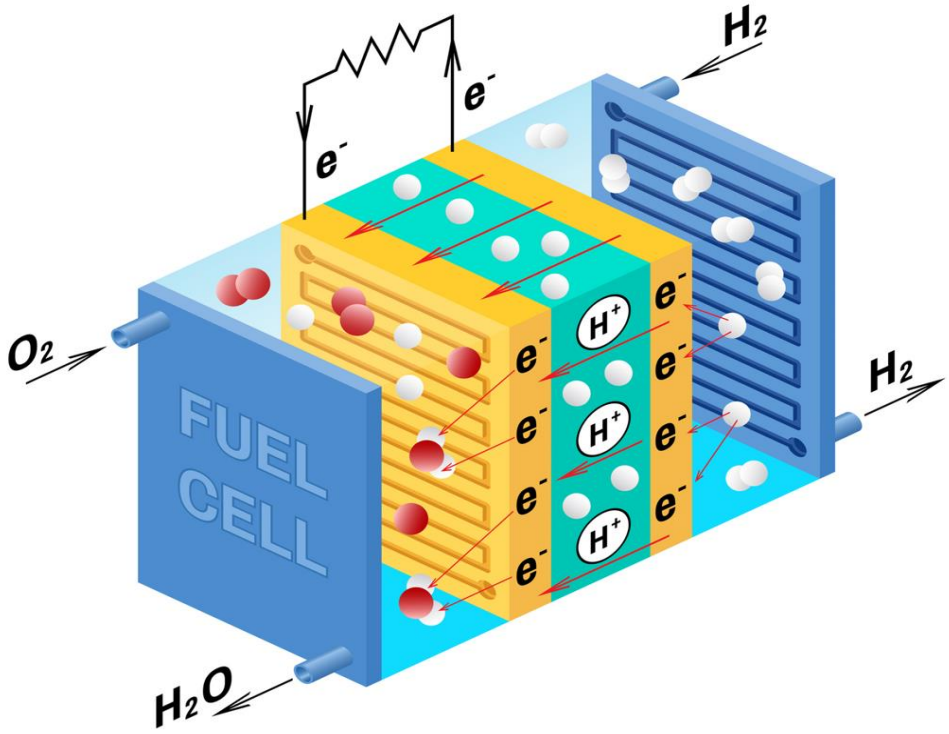

Fig. 1.4. Hydrogen fuel cell. In the anode, the hydrogen fuel is flowing into the chamber. The overall reaction is hydrogen combustion with oxygen. *Adapted from http://airbus.com/newsroom.*

In a typical MFC (**Fig. 1.5**), the anode and cathode chamber are separated by the proton exchange membrane (PEM)[15,16]. The exoelectrogenic bacteria are located on the anodic chamber and electrode. Under the anaerobic condition, the organic matter is first absorbed by the bacteria and proceed to anaerobic metabolism. During this process, the proton, carbon dioxide and electrons are produced. With extracellular electron transfer, the electrons are transferred to the anode electrode and being further transported through the outer circuit and finally reach the cathode. The cathode, where the electron acceptors are located, will combine with the incoming electrons. In general, the overall reaction of microbial fuel cell is still the same as the organic

matter aerobic consumption, but they are being realized through multiple steps separately by anodic bacteria and cathode electron acceptors[17].

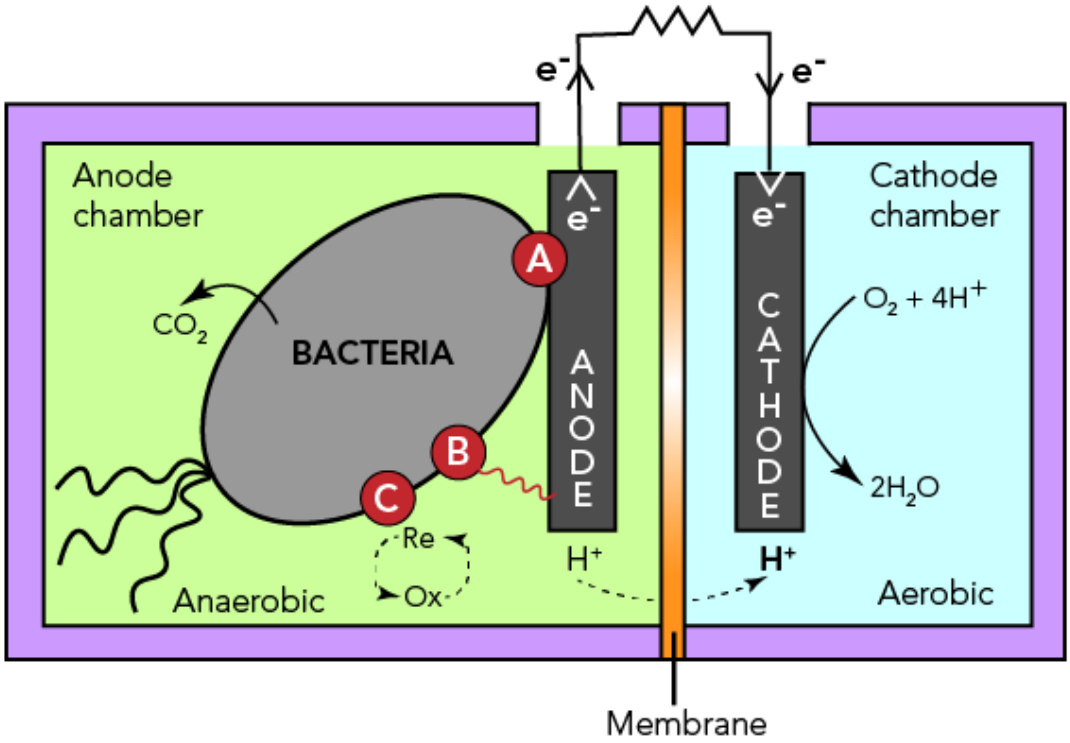

Fig. 1.5. A typical microbial fuel cell. The organic matter is oxidized by the bacterium. *Adapted from https://letstalkscience.ca/educational-resources/stem-in-context/microbial-fuel-cells.*

For a fuel cell with inorganic nanoparticle as the catalyst, the fuel may require high selectivity catalysts owing to different reaction mechanisms. Yet for bacteria with various of enzymes, they can take various of organic matters as the fuel resource and well overcome the selectivity problems. This will remind us of the waste water which contains organic mixtures. In the typical agricultural organic waste water, there are various kinds of organic waste such as carbohydrate and lipid. Although there are multiple ways to handle the organic waste mixture, this process may need more energy investing and the chemical energy restored in the organic waste are still abandoned and squandered (**Fig. 1.6**). With the microbial fuel cell as a mutual-beneficial method, we can well turn

the organic waste into the electricity power resource without any more energy investment[18]. According to the report, the total amount of energy restored in the organic waste water can be as large as 9 GW, which is about 9% of the electricity needed by the entire U.S. in one year[19].

Fig. 1.6. Typical structures of wastewater treatment, which need more energy investment to the whole system to get rid of the waste matter. *Adapted from https://en.wikipedia.org/wiki/Wastewater_treatment.*

However, despite significant efforts have been made to improve the microbial fuel cell performance and related electrode materials, the MFCs output are still too low to meet the practical level utilization. The output power density of MFCs to date has hit a plateau and rarely exceeds 3 W/m^2, which is likely due to limited efficiencies in transmembrane and extracellular electron transfer process[20,21]. More importantly, it is significant to study and expand the single exoelectrogenic bacterium level of performance through *in-situ* monitoring and modification to probe and address the essence of low MFCs performance.

1.3 Overview of the dissertation

In this dissertation, I will focus on the exoelectrogenic bacteria *Shewanella* and its cooperating with various of inorganic materials such as nano-devices and nanoparticles. In *Shewanella*-nano-devices hybrids, the current output features and cell density can be both *in-situ* monitored and studied. And by further anchoring the nanoparticles into the *Shewanella* membrane structures and related biofilms, we can realize the performance boosting to a new recorded level.

In chapter 2, we developed and applied a novel methodology to study the EET, metabolic activity status and behaviors of microbes for maximal current production with real time *in-situ* microscope observation. The dissimilatory extroelectrogenic bacteria *Shewanella oneidensis* MR-1 wild type (WT) and its mutant cells (Δbfe and ΔmtrC/ΔomcA) are the model organisms we study to understand exoelectrogenic biofilm growth, metabolism rate, and behavior for maximal current production. Our goal is to specify the various mechanisms of EET in MR-1and its mutant cells utilized by the bacteria under different conditions.

In chapter 3, we reported a rational strategy to boost the transmembrane and extracellular electron transfer processes significantly in *Shewanella* biofilms loaded on reduced graphene oxide/silver nanoparticle (rGO/Ag) scaffolds. Our systematic studies show that the rGO/Ag can release positively charged silver ions, which facilitate *Shewanella* attachment to rGO/Ag scaffold to form dense biofilms, while at the same time produce transmembrane and outer-membrane Ag nanoparticles to form the *Shewanella*-Ag hybrids, with greatly enhanced transmembrane and extracellular electron transfer efficiency to improve the bacteria turn-over frequency (TOFs) and boost the overall MFC performance. The resulting MFCs with the rGO/Ag anode can output a

current density of 38.5 A/m^2, a power density of 6.63 W/m^2 and a Coulombic efficiency of 81%, greatly outperforming the best *Shewanella* MFCs reported to date.

In chapter 4, considering the better metal ion releasing ability from Cu owning to the lower oxidation potential, we synthesized and fabricated rGO/Cu electrode to expand our *Shewanella*-metal hybrids method. The resulting MFCs can output a current density of 25 A/m^2, a power density of 4.5 W/m^2 and a Coulombic efficiency of 72%,

In chapter 5, I will make a conclusion based on the bacteria-inorganic hybrids and also draw a prospective to the future direction of related topics.

1.4 References

1. Whitman, W. B., Coleman, D. C. & Wiebe, W. J. Prokaryotes: The unseen majority. *Proc. Natl. Acad. Sci. U. S. A.* **95**, 6578–6583 (1998).

2. Sanders, M. E. Probiotics: Considerations for human health. *Nutr. Rev.* **61**, 91–99 (2003).

3. Legras, J. L., Merdinoglu, D., Cornuet, J. M. & Karst, F. Bread, beer and wine: Saccharomyces cerevisiae diversity reflects human history. *Mol. Ecol.* **16**, 2091–2102 (2007).

4. Kanakoudis, V. *et al.* Determining a socially fair drinking water pricing policy: The Case of Kozani, Greece. *Procedia Eng.* **162**, 486–493 (2016).

5. Logan, B. E. Exoelectrogenic bacteria that power microbial fuel cells. *Nat. Rev. Microbiol.* **7**, 375–381 (2009).

6. Venkateswaran, K. *et al.* Polyphasic taxonomy of the genus *Shewanella* and description of *Shewanella oneidensis* sp. nov. *Int. J. Syst. Bacteriol.* **49**, 705–724 (1999).

7. Ross, D. E. *et al.* Characterization of protein-protein interactions involved in iron reduction by *Shewanella oneidensis* MR-1. *Appl. Environ. Microbiol.* **73**, 5797–5808 (2007).

8. Bird, L. J., Bonnefoy, V. & Newman, D. K. Bioenergetic challenges of microbial iron metabolisms. *Trends Microbiol.* **19**, 330–340 (2011).

9. White, G. F. *et al.* Rapid electron exchange between surface-exposed bacterial cytochromes and Fe(III) minerals. *Proc. Natl. Acad. Sci. U. S. A.* **110**, 6346–6351 (2013).

10. El-Naggar, M. Y. *et al.* Electrical transport along bacterial nanowires from *Shewanella oneidensis* MR-1. *Proc. Natl. Acad. Sci.* **107**, 18127–18131 (2010).

11. Pirbadian, S. *et al. Shewanella oneidensis* MR-1 nanowires are outer membrane and periplasmic extensions of the extracellular electron transport components. *Proc. Natl. Acad. Sci. U. S. A.* **111**, 12883–12888 (2014).

12. Lygeros, J. *et al.* Stochastic hybrid modeling of DNA replication across a complete genome *Proc. Natl. Acad. Sci. U. S. A.* **106**, 9535 (2009).

13. Wang, C. Y. Fundamental models for fuel cell engineering. *Chem. Rev.* **104**, 4727–4765 (2004).

14. Cui, C. H., Li, H. H. & Yu, S. H. Large scale restructuring of porous Pt-Ni nanoparticle tubes for methanol oxidation: A highly reactive, stable, and restorable fuel cell catalyst. *Chem. Sci.* **2**, 1611–1614 (2011).

15. Rabaey, K. & Verstraete, W. Microbial fuel cells: Novel biotechnology for energy generation. *Trends Biotechnol.* **23**, 291–298 (2005).

16. Lu, L. *et al.* Wastewater treatment for carbon capture and utilization. *Nature Sustainability* **1**, 750–758 (2018).

17. Bruce E. Logan, Bert Hamelers, Ren éRozendal, Uwe Shroder, Jurg Keller, Stefano Freguia, Peter Aelterman, W. V. and K. R. Critical Review Microbial Fuel Cells : Methodology and Technology. *Environ. Sci. Technol.* **40**, 5181–5192 (2006).

18. Logan, B. E. & Regan, J. M. Electricity-producing bacterial communities in microbial fuel cells. *Trends Microbiol.* **14**, 512–518 (2006).

19. Logan, B. E. & Rabaey, K. Conversion of wastes into bioelectricity and chemicals by using microbial electrochemical technologies (Science (2012) (686)). *Science.* **339**, 906 (2013).

20. Zuo, J., Cui, L., Fan, M. & Song, W. Production of electricity from artificial wastewater using a single chamber microbial fuel cell. *Taiyangneng Xuebao/Acta Energiae Solaris Sin.* **28**, 320–323 (2007).

21. Wang, R. *et al.* FeS_2 nanoparticles decorated graphene as microbial-fuel-cell anode achieving high power density. *Adv. Mater.* **30**, 1–7 (2018).

Chapter 2: Novel Methodology for the Study of Bacterial Extracellular Electron Transport Mechanism and Metabolic Activity Status

2.1 Introduction

The ability of dissimilatory metal-reducing bacteria (DMRB) to oxidize the organic matters and transfer free electrons from microorganisms to mineral surface or electrodes during metabolism generates the electricity production in microbial fuel cells (MFCs).[1–7] Also, the extracellular electron transport (EET) mechanisms have been explored by different methods, mostly through electricity production of biofilms in MFCs[8]. Although several studies trying to address the conductivity measurement by using conducting atomic force microscope (AFM) or semiconductor device with dead/dry cells[9–15], those methods could only monitor the electricity production or conductivity in biofilms. The correlation between bacteria behaviors, metabolic activities and electricity production in biofilms or down to single cell level remain unclear. In addition, cell staining is still the most widely used technique for bacteria behaviors investigation and cell growth observation under fluorescent microscope. However, the toxicity of the dye in cell staining is still a concern.[16]

In this work, we developed and applied a novel methodology to study the EET, metabolic activity status and behaviors of microbes for maximal current production with real time *in-situ* microscope observation. The dissimilatory metal-reducing bacteria (DMRB) *Shewanella oneidensis* MR-1wild type (WT) and its mutant cells are the model organisms we study to understand exoelectrogenic biofilm growth, metabolism rate, and behavior for maximal current production. Our goal is to specify the various mechanisms of EET in MR-1and its mutant cells utilized by the bacteria under different conditions.

2.2 Experimental and methods

Strains and growth conditions

Shewanella oneidensis MR-1 strains wild type (WT), Δ*omcA*/Δ*mtrC*, and Δ*bfe* were used in this study. All chemicals were purchased from Sigma-Aldrich unless otherwise stated. Strains were cultured in LB broth overnight to stationary phase under shaking at 30 °C. The cells from this culture were pelleted via centrifugation at 2300*g* for 5 minutes, washed twice, and finally resuspended in a chemically defined medium ("nanowire medium"). The culture in the final nanowire medium was grown again to mid-log phase (OD_{600} ~ 0.5-0.7) under shaking at 30 °C. The culture was then diluted to OD_{600} ~ 0.02 and injected into a sterile flow cell containing the same medium.

The base nanowire medium contained (per liter of deionized water) 9.07 g of PIPES buffer, 3.4 g of sodium hydroxide, 1.5 g of ammonium chloride, 0.1 g of potassium chloride, 0.6 g of sodium phosphate monobasic monohydrate, 60 mM of 60% (v/v) sodium DL-lactate solution as an electron donor, 10 mL of 100× amino acids stock solution, and 10 mL of 100× minerals stock solution. This base medium was adjusted to an initial pH of 7.2 using HCl and NaOH and then sterile filtered using a 0.22 μm vacuum driven disposable bottle top filter (Millipore). Finally, before the medium was used, 0.5 mL of 100 mM ferric NTA stock solution was added per liter of medium. For media designated as "1× vitamins," 1 mL of 1000× vitamins stock solution was added per liter of medium; for media designated as "0× vitamins," the vitamins stock solution was not added. 1× vitamins nanowire medium was used for centrifugation, washing, resuspension, and regrowth steps, while both 1× and 0× vitamins nanowire media were used for flow cell experiments, depending on the desired condition.

The 100× amino acids stock solution contained (per liter of deionized water) 2 g of L-glutamic acid, 2 g of L-arginine, and 2 g of DL-serine. The 100× minerals stock solution contained (per liter of deionized water) 1.5 g of nitrilotriacetic acid, 3 g of magnesium sulfate heptahydrate, 0.5 g of manganese sulfate monohydrate, 1 g of sodium chloride, 0.1 g of ferrous sulfate heptahydrate, 0.1 g of calcium chloride dihydrate, 0.1 g of cobalt chloride hexahydrate, 0.13 g of zinc chloride, 10 mg of cupric sulfate pentahydrate, 10 mg of aluminum potassium disulfate dodecahydrate, 10 mg of boric acid, 25 mg of sodium molybdate dihydrate, 24 mg of nickel chloride hexahydrate, and 25 mg of sodium tungstate. The 1000× vitamins stock solution contained (per liter of deionized water) 20 mg of biotin, 20 mg of folic acid, 100 mg of pyridoxine hydrochloride, 50 mg of riboflavin, 50 mg of thiamine hydrochloride, 50 mg of nicotinic acid, 50 mg of D-pantothenic acid hemicalcium salt, 1 mg of vitamin B12, 50 mg of P-aminobenzoic acid, and 50 mg of DL-α-lipoic acid. The 100 mM ferric NTA stock solution contained (per 100 mL of deionized water) 1.64 g of sodium bicarbonate, 2.56 g of nitrilotriacetic acid (NTA) trisodium salt, and 2.7 g of ferric chloride hexahydrate. All stock solutions were sterile filtered prior to use.

Flow cell experiments

Flow cells were purchased from ibidi (Product name: sticky--Slide VI 0.4). A modified coverslip was pressed onto the flow cell adhesive to form the channels. The prepared flow cell was connected to a syringe and waste container using male Luer elbow connectors (ibidi), male Luer integral lock ring to 1.6 mm barb adapters (Value Plastics DBA Nordson Medical), an in-line Luer injection port (ibidi), female Luer to 1.6 mm barb adapters (Value Plastics DBA Nordson Medical), and Silastic silicon tubing of inner diameter 1.57 mm and outer diameter 3.18 mm (Dow Corning). The flow cell system was sterilized by flowing 70% ethanol by hand and letting the system sit

without flow for ~30 min. The sterilized system was then flushed with autoclaved, deionized water at a flow rate of 5 mL/h using a syringe pump (KD Scientific or Harvard Apparatus) and allowed to sit for ~2 h. Prior to inoculation of the bacteria into the flow cell, the flow cell system was flushed with flow cell media. 1 mL of bacteria culture was injected into the flow cell and allowed to incubate for 10 min on the heating stage at 30 °C. Then, the flow cell was flushed with flow cell media at 30 mL/h to wash away cells that had not adhered to the surface. For these experiments, data were collected using a flow rate of 3 mL/h and total flow time of ~45 h.

Data acquisition

Images were taken using two microscope systems. The first system was an Olympus IX81 microscope with an Andor iXon EMCCD camera (image size of 1024 × 1024 pixels and pixel size of 0.13 μm/pixel). The second system was an Olympus IX83 microscope with an Andor Neo sCMOS camera (image size of 2048 × 2048 pixels and pixel size of 0.065 μm/pixel). Both systems were controlled using IQ software (Andor) and were equipped with 100× oil objectives and Zero Drift Correction autofocus systems. Bright field images were taken every 10 s (30 ms exposure time). Two fluorescence images were also taken every 5 min (either 100 ms or 250 ms exposure times) using a Lambda LS (Sutter Instrument) xenon arc lamp and either a GFP or TRITC filter. Acquisition continued for a total recording time of ~45 h.

Prior to inoculation of bacteria, two types of background images were taken. The first type involved the in-focus surface (with varying degrees of focus) without bacteria, and the second type involved an out-of-focus image without the surface or bacteria. The first type of background image helped to reduce artifacts due to the surface patterns or defects, and the second type helped to reduce artifacts due to defects in the light path.

For imaging nanowires, the lipophilic styryl dye FM 4-64 FX (Life Technologies), diluted to 0.25 μg/mL with nanowire media, was injected into the flow cell and incubated for 5~10 min. Then, a fluorescence (mCherry filter, 500 ms exposure time) Z-scan (±1.5 μm from the imaging plane every 0.1 μm) was taken to image the presence or absence of nanowires stained with FM 4-64 FX. This process was repeated several times to confirm the presence or absence of nanowires.

Image and data analysis

The image analysis algorithms and software are adapted from methods previously described and written in MATLAB R2015a (MathWorks). First, all raw bright-field images were processed using a sequence of background correction, intensity normalization, Gaussian and edge filters, and Otsu thresholding to generate binary images, which contained main features of bacteria. The background correction step included cross-correlations of the raw images with images taken of the surface without bacteria; this allowed the surface patterns to be mostly ignored by subsequent analyses and the images to be corrected for spatial drift. The resulting binary images were used to calculate the area covered by bacteria on the surface (either on or off the pattern) over time. A linear interpolation step was then performed to ensure that the image and electrochemical data had the same time scale.

Fabrication of the Au electrochemical device

Typically, a PMMA (A8, MicroChem Corp.) film was prepared by spin coating on the substrate (glass cover slide) surface with pre-patterned Au electrodes (Ti/Au, 10/60 nm) and pre-patterned Au electrodes (Ti/Au, 5/10 nm). E-beam lithography was then used to open windows on PMMA, which created desired patterns on the substrate. To eliminate the influence of electrolyte and to avoid electrochemical reactions on the metal electrodes, another layer of PMMA (~ 500-

nm thick, electrochemically inert) was then deposited on the Au pattern device with spin coating. A smaller window that only exposes Au electrode was opened by e-beam lithography. The final device, with exposed Au electrode protected electrodes was used for in-device electrochemistry and in situ electrical transport spectroscopy measurement.

In-device I-t measurement

All electrochemical data were recorded using a SMU (Agilent B2902a) electrochemical workstation with a three-electrode electrochemical flow cell containing an Ti/Au working electrode, a platinum-wire counter electrode, and an Ag/AgCl reference electrode. The Au square pattern (50 um x 60 um) was prepared by thermal evaporation. In a typical in-device CV measurement, the scan rate is 50 mVs^{-1}. The SMU channel was used to supply a small potential (50 mV) on working electrodes (working electrode is grounded) and collecting the corresponding electrochemical current.

Half-cell microbial fuel cell experiment

The three electrodes are placed in a three-neck flask. The working electrode is carbon paper or carbon paper/rGO or carbon paper/rGO/Ag. The reference electrode is 1 M KCl Ag/AgCl electrode, and the counter electrode is platinum wire. After adding all the solutions, the entire system is purged with ultra-pure N_2 gas for 30 min to remove dissolved oxygen. In a typical current-time (*I-t*) measurement, a positive potential (200 mV vs. reference electrode) is added on the working electrode and the corresponding electrochemical current is recorded.

Full cell microbial fuel cell experiment

The H-shaped two-chamber MFC is constructed by connecting two 120 ml chambers with a proton exchange membrane (PEM) Nafion 211 separator. The diameter of the chamber channel is

5.5 cm. The cathode is carbon cloth (2 cm × 4 cm) coated with 40% Pt/C with oxygen purging. Before the tests, two sterilization steps are conducted to ensure the device is fully sterilized. Before constructing the devices, all the plastic chambers are soaked in aqueous detergent solution, and sufficiently rinsed with deionized water. After the devices and membranes are fully constructed, the entire device is immersed into boiling water for 15 min for further sterilization. Before the test, the anodic solution is purged with pure nitrogen gas for 30 min to remove the dissolved oxygen. The anodic chamber is tightly sealed to maintain the anaerobic condition during MFC operation. All MFC experiments are operated at ~30 °C. At MFC steady state, the polarization curves are obtained by varying the external resistor. The output voltage is recorded with a multi-meter. The output current is calculated from Ohm's Law: $I=V/R$ (R is the value of external resistor). The output power is calculated by $P=IV=V^2/R$. For long-standing tests and the EIS tests, the cathode solution is changed to potassium ferricyanide ($K_3[Fe(CN)_6]$, 50 mM) and potassium chloride (KCl, 50 mM).

2.3 Results and discussion

Figure 2.1 schematically illustrates the *in-situ* electrochemical current measurement setup in the flow cell and electrode layout used for probing the electrical transport in microbial cells and biofilms. Au electrode was prepatterned on a cover slide glass using electron-beam lithography (EBL). A PMMA window was employed to define a testing window and exposure of electrodes to the microbial samples in the culture medium. The confined window also enables the precise control of the exact electrode area exposed to the microbial samples. This novel methodology provides us the ability to measure electron transport at the single-cell level as well as to monitor bacterial behavior and correlation between the electrochemical current and metabolic activity.[17]

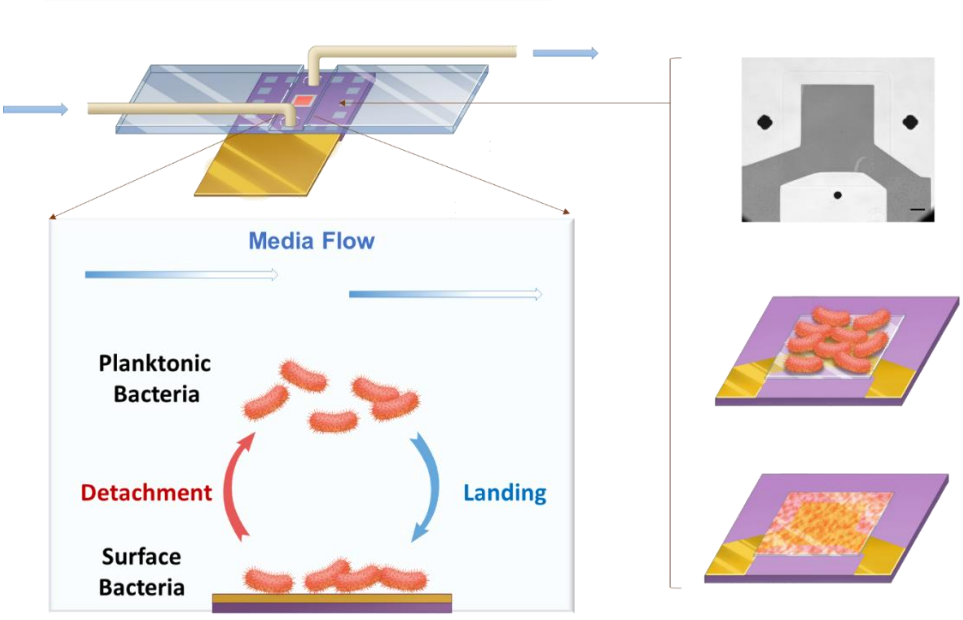

Figure 2.1 Schematic illustration of in-situ *Shewanella oneidensis* MR-1 electrochemical current measurements setup within flow cell. Scale bar is 10 μm.

Here, we demonstrated an electrochemical current measurement system with applying potential 50 mV (vs Ag/AgCl) and incubated with living WT, a double-deletion mutant of mtrC and omcA (ΔmtrC/ΔomcA) and a deletion mutant lacking the function of FMN secretion (Δbfe) on the designed Au electrodes in a microfluidic flow cell. As shown in **figure 2.2**, the real-time bright field optical images clearly show the different cell growth rates between WT, ΔmtrC/ΔomcA and Δbfe. Interestingly, the form ΔmtrC/ΔomcA mutant cells were fully covered on designed Au electrode after 30 hr and started to form a biofilm.

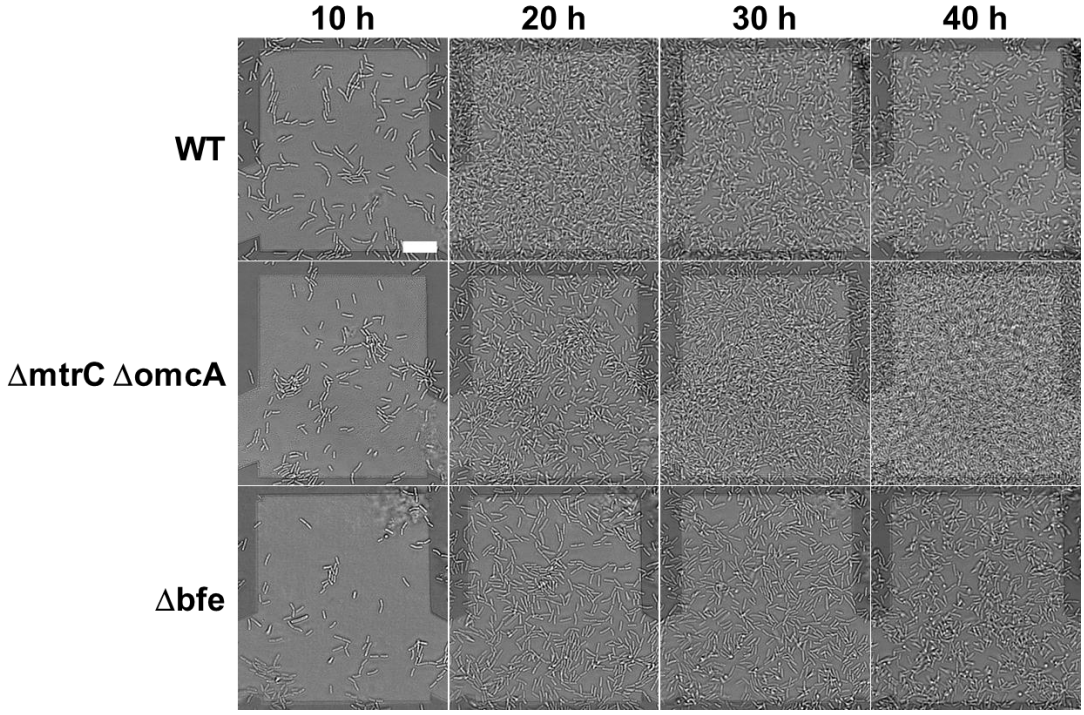

Figure 2.2 Representative time-lapse images of *Shewanella oneidensis* MR-1, ΔmtrC/ΔomcA and Δbfe are incubated with Au substrate in flow cell for 10 hr, 20 hr, 30 hr and 40 hr. Scale bar is 10 μm.

Figure 2.3a illustrates the surface cell density of WT**,** ΔmtrC/ΔomcA and Δbfe on designed Au electrode. While the growth rate became stabilized on WT and Δbfe after about 20 hr, it is remarkably to see the Δbfe mutant cells kept growing and started to grow along z-axis after 34 hr. Since the designed Au electrode was totally covered by Δbfe mutant cells after 34 hr, the surface cell density of Δbfe mutant cells was stabilized after 34 hr. Interestingly, although the highest surface cell density were fund on ΔmtrC/ΔomcA mutant cells, the current density of ΔmtrC/ΔomcA is ~ 5 x 20^{-6} nA/μm^2 which is about 2 to 3 orders lower than WT and Δbfe (**Fig 2.2b**). Moreover, the WT and Δbfe have similar surface cell surface at 40 hr, but the current density Δbfe is about 2

orders higher than WT. By comparing the observations between electrochemical current and surface cell density, it shows the protein c-type cytochrome mtrC and omcA are the major factors that significantly affect electricity production and the deletion of the MET pathway (FMN deletion) can also enhanced the electricity production. However, the WT didn't express highest electricity current, the possible hypothesis is that there is coexisting with DET and MET pathway in WT, the free electrons could transfer through either DET or MET pathway. However, the MET pathway seems like limiting electron transfer, so the electrochemical current in WT is lower than Δbfe. The *in-situ* real time electrochemical current measurement in microfluidic flow cell can also use for investigating the electricity production from each single cell (**Fig 2.3c**).

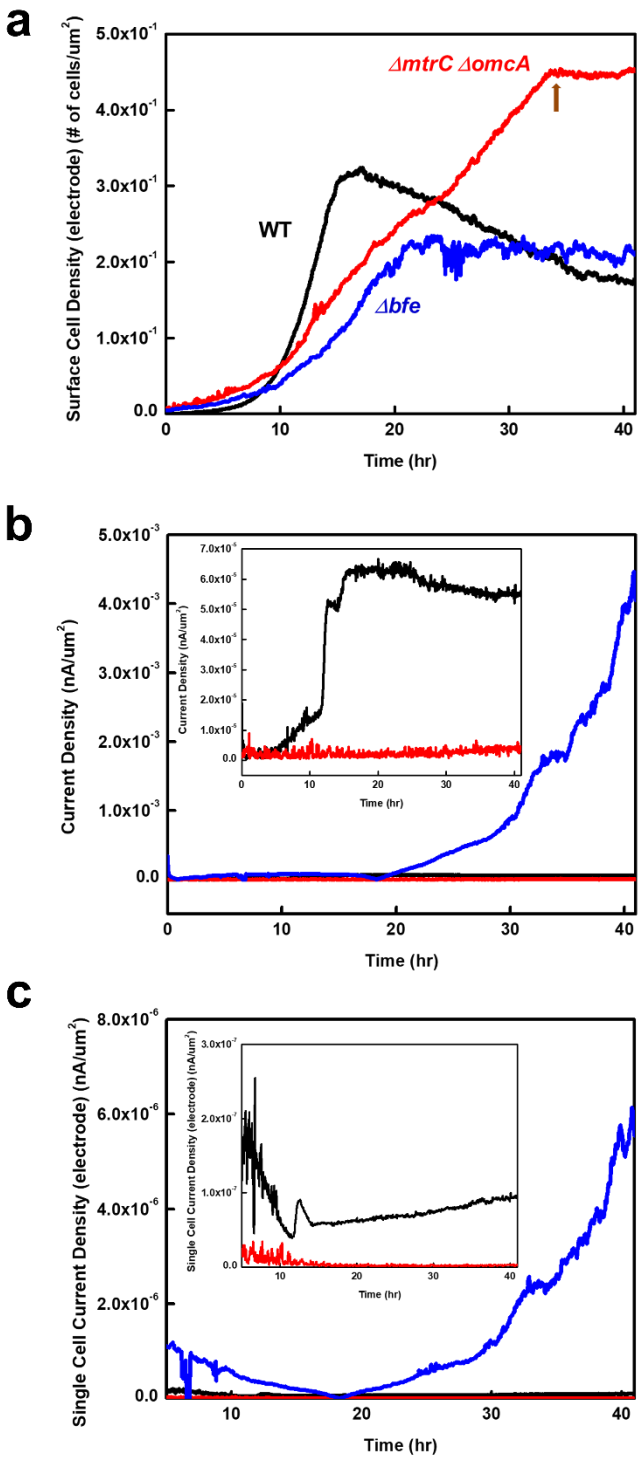
a
Surface Cell Density (electrode) (# of cells/um2)
5.0x10-1
4.0x10-1
3.0x10-1
2.0x10-1
1.0x10-1
0.0
0
10
20
30
40
Time (hr)
ΔmtrC ΔomcA
WT
Δbfe
b
Current Density (nA/um2)
5.0x10-3
4.0x10-3
3.0x10-3
2.0x10-3
1.0x10-3
0.0
0
10
20
30
40
Time (hr)
Current Density (nA/um2)
7.0x10-4
6.0x10-4
5.0x10-4
4.0x10-4
3.0x10-4
2.0x10-4
1.0x10-4
0.0
0
10
20
30
40
Time (hr)
c
Single Cell Current Density (electrode) (nA/um2)
8.0x10-6
6.0x10-6
4.0x10-6
2.0x10-6
0.0
10
20
30
40
Time (hr)
Single Cell Current Density (electrode) (nA/um2)
3.0x10-7
2.0x10-7
1.0x10-7
0.0
10
20
30
40
Time (hr)

Figure 2.3 Electrochemical measurements of living MR-1, ΔmtrC/ΔomcA and Δbfe in flow cell. Representative **a**, Surface cell density **b**, Current density and **c**, Single cell current density of living MR-1, ΔmtrC/ΔomcA and Δbfe as function of incubation time on the device.

Fig 2.4 demonstrates the correlation between the current density and surface cell density in living WT (**Fig 2.4a**), **Δ**bfe (**Fig 2.4b**) and ΔmtrC/ΔomcA (**Fig 2.4c**) of as the function of incubation time. Interestingly, there are three different presentations shown at WT, **Δ**bfe and ΔmtrC/ΔomcA. First of all, cell growth and electrochemical current generation shows on WT are similar. After cell growth of Δbfe became stabilized, the electrochemical current started to increase rapidly. However, the cells kept growing and there was no electrochemical current shown on Δmtrc/ΔomcA. Based on those results, the cell growth is highly correlation to electrochemical current generation. According to previously studies, the oxidation of formate is limiting reactant for cell growth. The proton, pair of electrons and carbon dioxide are produced during the oxidation of $formate^-$, it enhances cell growth rate and also consumes the free electrons to gain ATP for cell growing.[18,19] There is no DET pathway and also probably the rate of MET is too slow in Δmtrc/ΔomcA mutant cells, so the cell kept growing without electrochemical current generation.

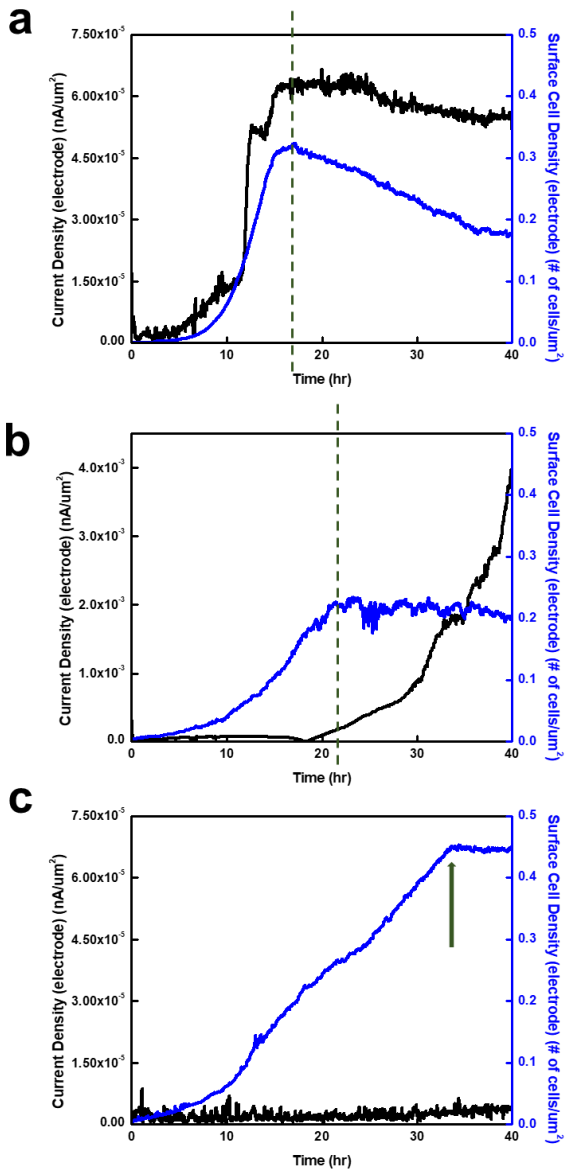

Figure 2.4 Electrochemical measurements of living MR-1, ΔmtrC/ΔomcA and Δbfe in flow cell. Representative current density and surface cell density of living **a**, MR-1 **b**, Δbfe and **c**, ΔmtrC/ΔomcA as function of incubation time on the device.

In addition, this result is also confirmed by the similar cyclic voltammetry (CV) characteristics of WT and its mutant cells on Au designed electrodes (**Fig. 2.5**), where an obvious

increase was observed in anodic current at about -0.035V (vs. Ag/AgCl, the electrochemical potential for the oxidation of general electron donors such as acetate) at Δbfe which indicates the free electrons transfer through c-type cytochrome (DET pathway).[20] It is also a good strategy to study the bacteria metabolic activities by CV measurement.

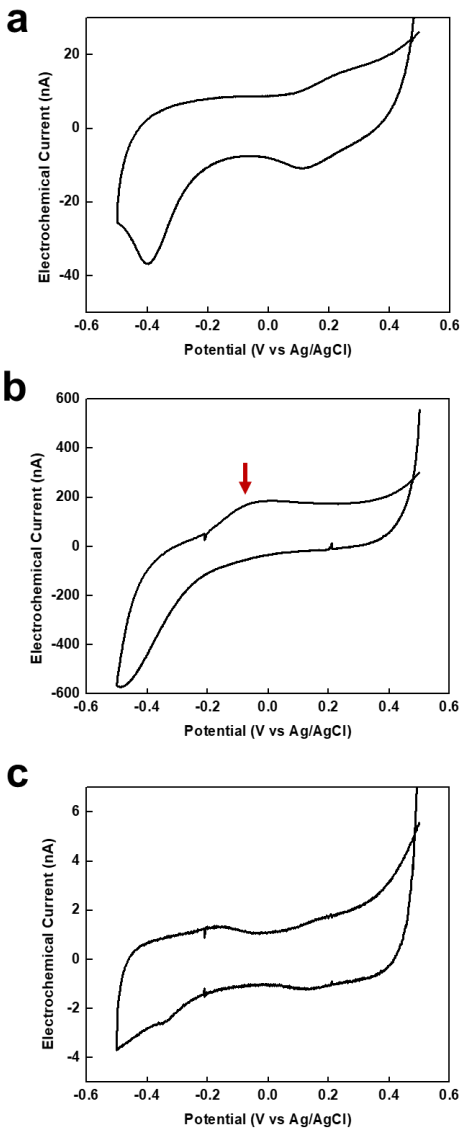

Fig 2.5 Electrochemical measurements of living WT, ΔmtrC/ΔomcA and Δbfe in flow cell. Representative electrochemical current density-potential (vs Ag/AgCl) transport characteristics of living **a**, MR-1 **b**, Δbfe and **c**, ΔmtrC/ΔomcA, acquired after 40 h on-chip incubation.

Based on the on-chip tests of MR-1 and mutants, we can easily predict that although the mutant may increase from the aspect of cell density, their overall performance is still lower than the wild type because of lack of intrinsic membrane protein channel. To further elucidate and proof our prediction, we conduct the microbial fuel cell (MFC) tests based on *Shewanella* and related mutants. The MFC is constructed based on the exoelectrogenic feature, in which the bacteria are acting like the catalyst to help consume the organic matter and produce the extracellular electrons. Through the connection of bio-anode and cathode, the electrons will go through the outer circuit to form a fuel cell.

For MFC tests of MR-1**,** Δbfe and ΔmtrC/ΔomcA, we first conduct the primary electrochemical tests. We simply use the most commercially used anode electrode material---carbon paper as the solitary bio-anode. In the 3-electrode system, the current collected by the working electrode (in this case, also the anode) is recorded as the *I-t* curves (**Fig. 2.6**). It is clear that even in the MFC primary tests, the current density of wild type (MR-1, 0.65 A/m^2) is still higher than the Δbfe (0.34 A/m^2) and ΔmtrC/ΔomcA (0.18 A/m^2).

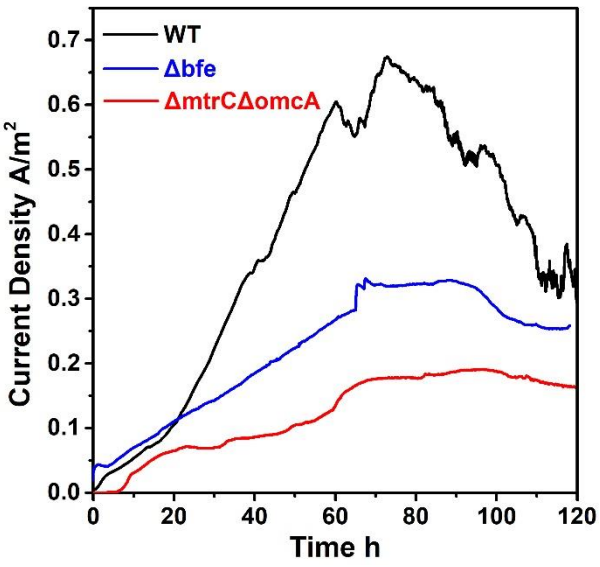

Fig 2.6 Microbial fuel cell measurements of living WT, ΔmtrC/ΔomcA and Δbfe with the electrode of carbon paper. Representative electrochemical current density-potential (vs Ag/AgCl) transport characteristics of living MR-1 (black), Δbfe (blue) and ΔmtrC/ΔomcA (red), acquired after 120 h incubation.

Based on the result of primary MFC tests, we further constructed the full cell test where there are anode and cathode separately distributed in the H-shape cell (**Fig. 2.7**). Our full cell test also matches well with our on-chip tests and *I-t* tests. For carbon paper as the anode electrode, the MR-1 (0.5 W/m^2) power generation is higher than Δbfe (0.32 W/m^2) and ΔmtrC/ΔomcA (0.23 W/m^2).

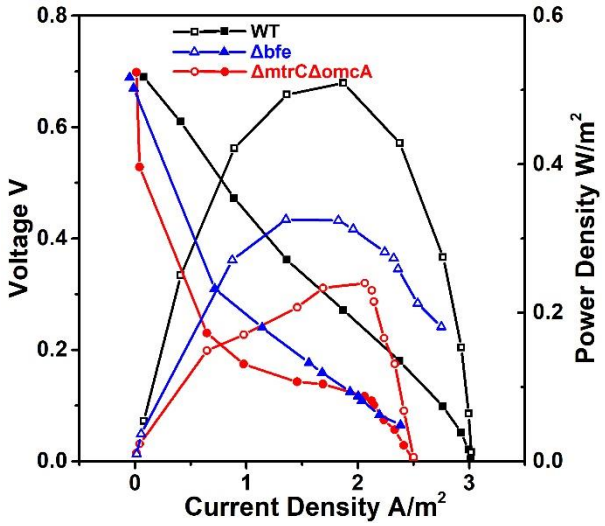

Fig 2.7 Microbial fuel cell full cell measurements of living WT, ΔmtrC/ΔomcA and Δbfe.

2.4 Summary

We have demonstrated nanoelectronic fabrication and measurement to elucidate the origin of the electrical conducting current from *Shewanella oneidensis* MR-1, ΔmtrC/ΔomcA and Δbfe. The electrical characteristics of living MR-1, ΔmtrC/ΔomcA and Δbfe were obtained under physiological conditions together with *in situ* real time optical imaging and other on-chip measurement approaches without artificial coloration. Based on those electrochemical current shown on MR-1, ΔmtrC/ΔomcA and Δbfe, the different electron transport pathway was discussed. This methodology reported in this study could explore more fundamental and theoretical studies on EET pathway and also metabolic activities status. Our electrochemistry model provides valuable insights into the elucidation of EET mechanisms by providing experimental supports for the currently proposed “direct electron transfer” mechanism is major factor that unifies the EET mechanism in *Shewanella oneidensis* MR-1.

2.5 References

1. Wang, H., Park, J.-D. & Ren, Z. J. Practical Energy Harvesting for Microbial Fuel Cells: A Review. *Environ. Sci. Technol.* **49**, 3267–3277 (2015).
2. Franks, A. E. & Nevin, K. P. Microbial fuel cells, a current review. *Energies* **3**, 899–919 (2010).
3. Logan, B. E. *et al.* Microbial fuel cells: Methodology and technology. *Environ. Sci. Technol.* **40**, 5181–5192 (2006).
4. Du, Z., Li, H. & Gu, T. A state of the art review on microbial fuel cells: A promising technology for wastewater treatment and bioenergy. *Biotechnol. Adv.* **25**, 464–482 (2007).
5. Pant, D., Van Bogaert, G., Diels, L. & Vanbroekhoven, K. A review of the substrates used in microbial fuel cells (MFCs) for sustainable energy production. *Bioresour. Technol.* **101**, 1533–1543 (2010).
6. Ge, Z., Li, J., Xiao, L., Tong, Y. & He, Z. Recovery of Electrical Energy in Microbial Fuel Cells. *Environ. Sci. Technol. Lett.* **1**, 137–141 (2014).
7. Logan, B. E. Exoelectrogenic bacteria that power microbial fuel cells. *Nat. Rev. Microbiol.* **7**, 375–381 (2009).
8. Malvankar, N. S. *et al.* Tunable metallic-like conductivity in microbial nanowire networks. *Nat. Nanotechnol.* **6**, 573–579 (2011).
9. Leung, K. M. *et al. Shewanella oneidensis* MR-1 bacterial nanowires exhibit p-type, tunable electronic behavior. *Nano Letters* **13**, 2407–2411 (2013).
10. El-Naggar, M. Y. *et al.* Electrical transport along bacterial nanowires from *Shewanella oneidensis* MR-1. *Proc. Natl. Acad. Sci.* **107**, 18127–18131 (2010).

11. Gorby, Y. A. *et al.* Electrically conductive bacterial nanowires produced by *Shewanella oneidensis* strain MR-1 and other microorganisms. *Proc. Natl. Acad. Sci.* **103**, 11358–11363 (2006).

12. Yang, Y., Xu, M., Guo, J. & Sun, G. Bacterial extracellular electron transfer in bioelectrochemical systems. *Process Biochem.* **47**, 1707–1714 (2012).

13. Polizzi, N. F., Skourtis, S. S. & Beratan, D. N. Physical constraints on charge transport through bacterial nanowires. *Faraday Discuss.* **155**, 43–61 (2012).

14. Pirbadian, S. & El-Naggar, M. Y. Multistep hopping and extracellular charge transfer in microbial redox chains. *Phys. Chem. Chem. Phys.* **14**, 13802 (2012).

15. Pirbadian, S. *et al. Shewanella oneidensis* MR-1 nanowires are outer membrane and periplasmic extensions of the extracellular electron transport components. *Proc. Natl. Acad. Sci.* **111**, 12883–12888 (2014).

16. Fried, J. *et al.* Effects of Hoechst 33342 on survival and growth of two tumor cell lines and on hematopoietically normal bone marrow cells. *Cytometry* **3**, 42–47 (1982).

17. Ding, M. *et al.* An on-chip electrical transport spectroscopy approach for in situ monitoring electrochemical interfaces. *Nat. Commun.* **6**, 1–9 (2015).

18. Kane, A. L. *et al.* Formate metabolism in *Shewanella oneidensis* generates proton motive force and prevents growth without an electron acceptor. *J. Bacteriol.* **198**, JB.00927-15 (2016).

19. Jensen, H. M., TerAvest, M. A., Kokish, M. G. & Ajo-Franklin, C. M. CymA and exogenous flavins improve extracellular electron transfer and couple it to cell growth in Mtr-Expressing *Escherichia coli*. *ACS Synth. Biol.* **5**, 679–688 (2016).

20. Xu, S., Jangir, Y. & El-Naggar, M. Y. Disentangling the roles of free and cytochrome-bound flavins in extracellular electron transport from *Shewanella oneidensis* MR-1. *Electrochim. Acta* **198**, 49–55 (2016).

Chapter 3: Boosting charge extraction efficiency in *Shewanella* biofilms with trans/outer-membrane silver nanoparticles

3.1 Introduction

Microbial fuel cells (MFCs) can directly convert chemical energy stored in many source of biodegradable organic matters to electrical energy through the microorganism metabolism [1,2]. The diverse bacteria species [3] and the wide range of fuels [4,5] makes the MFCs an attractive technology for renewable bioelectricity power generation from biomass and wastewater treatment[6]. For this reason, the MFCs and the relevant bacteria have attracted increasing attention from academic and industrial communities [7]. Among them, *Shewanella* is one of the most widely studied bacteria for bioremediation and environmental energy recovery due to its robust vitality in both aerobic and anaerobic environments [8] and its rich distribution in soil and seawater [9]. However, the current density and power density obtained from the typical *Shewanella* MFCs are generally too low for practical applications [4,10]. The low power output is generally limited by the bacterial anodes due to low bacterial loading capacity [6,11] and/or relatively poor extracellular electron transfer efficiency [12,13].

Considerable efforts have been devoted to improving the MFC anodic electrodes by increasing the bacteria loading capacity or enhancing the electrode conductivity [14]. Graphite [15] and carbon black [16] are commonly used as the biocompatible MFC anode materials. In particular, commercial carbon paper [17] and carbon cloth [18] have been broadly explored, since the carbon fiber structures can significantly increase the roughness for bacterial loading and retain structural and electrical connectivity. Additionally, 3D electrodes with mesoporous structures [19,20] could provide higher specific surface area and larger space for more bacteria loading. More recently, carbon nanomaterials such as graphene [21], carbon nanotubes [22–24] and their composites with non-carbon

materials [25] have been explored for reducing the charge transfer resistance of the anodic electrodes. However, despite considerable efforts with such strategies, the output power density of the MFCs to date has hit a plateau [8] and rarely exceeds 3 W/m^2, which is likely due to limited efficiencies in transmembrane and extracellular electron transfer process [26].

Within the bacteria in MFCs, the metabolic tricarboxylic acid cycles (TCA) in the bacteria cytoplasm produce electrons in the form of electron carriers (nicotinamide adenine dinucleotide, NADH), which transfers the electrons to quinones near the inner membranes to produce quinols [27]. The electrons stored in quinols can then cross the periplasm between the inner membrane and the outer membrane through the multistep hopping between the cytochrome redox centers. On the outer membrane, the electrons are transferred to the electrode surface through a series of direct or indirect extracellular electron transfer process [28–30]. Overall, the transmembrane and extracellular electron transfer processes generally involve sluggish electron hopping through redox centers in atypical conductors or through multiple redox cycles, which could severely limit the charge transfer efficiency. Therefore, to break through the power limit of the current MFCs, it is essential to design and to fabricate novel anodic electrodes that can fundamentally address these charge transfer limitations to efficiently deliver the metabolic electrons to the external electrodes [31,32].

Here, we report a rational strategy to boost the transmembrane and extracellular electron transfer processes significantly in *Shewanella* biofilms loaded on reduced graphene oxide/silver nanoparticle (rGO/Ag) scaffolds. Our systematic studies show that the rGO/Ag can release positively charged silver ions, which facilitate *Shewanella* attachment to rGO/Ag scaffold to form dense biofilms, while at the same time produce transmembrane and outer-membrane Ag nanoparticles to form the *Shewanella*-Ag hybrids, with greatly enhanced transmembrane and extracellular electron transfer efficiency to improve the bacteria turn-over frequency (TOFs) and

boost the overall MFC performance. The resulting MFCs with the rGO/Ag anode can output a current density of 38.5 A/m^2, a power density of 6.63 W/m^2 and a Coulombic efficiency of 81%, greatly outperforming the best *Shewanella* MFCs reported to date.

3.2 Experimental sections and methods

Synthesis of reduced graphene oxide/Ag nanoparticles (rGO/Ag) and rGO composites

Typically, 2 ml of graphene oxide (3 mg/ml) solution is mixed with 2 ml of silver nitrate ($AgNO_3$ 0.1 M) aqueous solution and 6 ml of DI water. 20 mg of sodium borohydride ($NaBH_4$) is dissolved in 10 ml DI water. Under vigorous stirring, the 10 ml $NaBH_4$ solution is added dropwise, slowly. After 10 min, the entire solution becomes dark black. Stirring is continued overnight at room temperature. The rGO/Ag composite is washed three times with the centrifuge and sonication with the DI water. Finally, the composite is dissolved in 10 ml ethanol for further use. For rGO, the entire process is the same except no $AgNO_3$ is added.

Fabrication of carbon paper/rGO/Ag nanoparticles and carbon paper/rGO anode

The carbon paper (CP) is cut into small pieces, 2 cm^2 (1 cm × 2 cm). 1 ml of the rGO/Ag solution is dropped on carbon paper to form a uniform layer. After that, the sample is dried in air. For carbon paper/rGO anode, the fabrication process and drying are the same.

Bacteria culture

Shewanella oneidensis MR-1 is first inoculated with 20 ml of LB solution. The entire flask together with the LB solution is put in a 30 ℃ shaker for at least 15 h (usually overnight). 200 μL of bacteria colonies are taken out and put in another flask containing 20 ml of fresh LB solution. Before any test, 5 ml of bacteria colonies are taken out, centrifuged and washed 3 times with *Shewanella* medium. The final bacteria solution's OD_{600} is about 1.0.

Shewanella medium ingredient

The *Shewanella* medium contains (per liter of deionized water): 9.07 g PIPES buffer ($C_8H_{18}N_2O_6S_2$), 3.4 g sodium hydroxide (NaOH), 1.5 g ammonium chloride (NH_4Cl), 0.1 g potassium chloride (KCl), 0.6 g sodium phosphate monobasic monohydrate ($NaH_2PO_4 \cdot H_2O$), 18 mM 60% (v/v) sodium DL-lactate ($C_3H_6O_3$)solution as the electron donor, 10 mL of 100× amino acids stock solution, and 10 mL 100× minerals stock solution. This base medium is adjusted to an initial pH of 7.2 using HCl and NaOH and then sterile filtered using 0.22 μm vacuum driven disposable bottle top filters (Millipore). Finally, before the medium is used, 0.5 mL 100 mM ferric NTA ($C_6H_6FeNO_6$) stock solution is added per liter of medium. The 100× amino acids stock solution contains (per liter of deionized water) 2 g L-glutamic acid ($C_5H_9NO_4$), 2 g L-arginine ($C_6H_{14}N_4O_2$), and 2 g DL-serine ($C_3H_7NO_3$). The 100× minerals stock solution contains (per liter of deionized water): 1.5 g nitrilotriacetic acid ($C_6H_9NO_6$), 3 g magnesium sulfate heptahydrate ($MgSO_4 \cdot 7H_2O$), 0.5 g manganese sulfate monohydrate ($MnSO_4 \cdot H_2O$), 1 g sodium chloride (NaCl), 0.1 g ferrous sulfate heptahydrate ($FeSO_4 \cdot 7H_2O$), 0.1 g calcium chloride dehydrate ($CaCl_2 \cdot 2H_2O$), 0.1 g cobalt chloride hexahydrate ($CoCl_2 \cdot 6H_2O$), 0.13 g zinc chloride ($ZnCl_2$), 10 mg cupric sulfate pentahydrate ($CuSO_4 \cdot 5H_2O$), 10 mg aluminum potassium disulfate dodecahydrate ($KAl(SO_4)_2 \cdot 12H_2O$), 10 mg boric acid (H_3BO_3), 25 mg sodium molybdate dehydrate (Na_2MoO_4), 24 mg nickel chloride hexahydrate ($NiCl_2 \cdot 6H_2O$), and 25 mg sodium tungstate (Na_2WO_4). All stock solutions are sterile filtered prior to use.

Half-cell microbial fuel cell experiment

The three electrodes are placed in a three-neck flask. The working electrode is carbon paper or carbon paper/rGO or carbon paper/rGO/Ag. The reference electrode is 1 M KCl Ag/AgCl

electrode, and the counter electrode is platinum wire. After adding all the solutions, the entire system is purged with ultra-pure N_2 gas for 30 min to remove dissolved oxygen. In a typical current-time (*I-t*) measurement, a positive potential (200 mV vs. reference electrode) is added on the working electrode and the corresponding electrochemical current is recorded.

Full cell microbial fuel cell experiment

The H-shaped two-chamber MFC is constructed by connecting two 120 ml chambers with a proton exchange membrane (PEM) Nafion 211 separator. The diameter of the chamber channel is 5.5 cm. The cathode is carbon cloth (2 cm × 4 cm) coated with 40% Pt/C with oxygen purging. Before the tests, two sterilization steps are conducted to ensure the device is fully sterilized. Before constructing the devices, all the plastic chambers are soaked in aqueous detergent solution, and sufficiently rinsed with deionized water. After the devices and membranes are fully constructed, the entire device is immersed into boiling water for 15 min for further sterilization. Before the test, the anodic solution is purged with pure nitrogen gas for 30 min to remove the dissolved oxygen. The anodic chamber is tightly sealed to maintain the anaerobic condition during MFC operation. All MFC experiments are operated at ~30 °C. At MFC steady state, the polarization curves are obtained by varying the external resistor. The output voltage is recorded with a multi-meter. The output current is calculated from Ohm's Law: I=V/R (R is the value of external resistor). The output power is calculated by $P=IV=V^2/R$. For long-standing tests and the EIS tests, the cathode solution is changed to potassium ferricyanide ($K_3[Fe(CN)_6]$, 50 mM) and potassium chloride (KCl, 50 mM).

Bacteria number determination

The bacteria numbers on different electrodes are determined with the combination of hemocytometer counting method and total nitrogen analysis method. In a typical hemocytometer

counting process, bacterial solutions after calibrated dilution are dripped on the hemocytometer counting chamber with the cover glass. The volume of a 1 mm grid is 1×10^{-4} ml. Total nitrogen analysis is conducted through HACH total nitrogen reagent set (high range, persulfate digestion method). The electrode after an MFC cycle is sonicated to break the biofilm from the electrode for nitrogen analysis.

Scanning electron microscope (SEM) measurement

After MFC testing, the entire anode with the biofilm is fixed by 2.5% glutaraldehyde ($C_5H_8O_2$) solution overnight at 4 °C and chemically dehydrated using gradient concentration ethanol aqueous solution (50, 70, 80, 90, and 95% each one, then 100% twice). The sample was dried in the vacuum chamber and finally sputter-coated gold for further SEM imaging.

Transmission electron microscope (TEM) measurements

After MFC testing, the bacterial solution is taken out, centrifuged and fixed by 2.5% glutaraldehyde ($C_5H_8O_2$) solution overnight at 4 °C and 2% osmium tetroxide (OsO_4) aqueous solution at 4 °C for 4 h. After fixation, the bacteria pellet is chemically dehydrated using gradient concentration of ethanol (50, 70, 80, 90, and 95% once each, then 100% twice) and 100% acetone. The bacteria pellet is finally embedded in the resin (Araldite 502) and polymerized in the oven at 60 ℃ for at least 36 h. Ultrathin sections of 70 nm are cut by an ultratome and deposited on carbon coated copper grids for TEM imaging.

Electrochemical surface area (ECSA) measurement

The electrochemical surface area (ECSA) of our samples is determined by testing the double layer capacitance (C_{dl}), in which C_{dl} is linearly proportional to the active surface area in the electrochemical capacitor research. In this process, cyclic voltammetry (CV) measurements were

conducted in the medium buffer solution without bacteria within the non-faradaic potential range (0.1-0.2 V vs. Ag/AgCl), which is dominated by surface adsorption/desorption. Then C_{dl} can be calculated by plotting the current difference between anodic and cathodic sweep ($\Delta J = J_a - J_c$) at 0.15 V against the different scan rate, where the slope is twice that of C_{dl}. In order to determine the exact value of the ECSA, we also determined the C_{dl} of a flat surface (e.g., glassy carbon electrode) with known geometry and surface area (0.196 cm^2).

Electrochemical impedance spectroscopy (EIS) measurement

For the R_{ct} of different electrodes without the bacteria, the measurement is conducted in a three-neck flask with bacteria buffer medium and 50 mM $K_3[Fe(CN)_6]$. The three electrodes carbon paper, rGO, and rGO/Ag are set as working electrodes. The Pt wire and Ag/AgCl are set as the counter electrode and the reference electrode, respectively. EIS is measured within the frequency range of 10^5 to 0.5 Hz at the voltage of 0.2 V vs RHE. For the full MFC, the EIS test is conducted after 2 days of MFC setup. The cathode is the potassium ferricyanide ($K_3[Fe(CN)_6]$, 50 mM) and potassium chloride (KCl, 50 mM). The anode is set as the working electrode and the cathode is connected with both the counter and reference electrode.

Confocal laser scanning microscopy (CLSM) measurement

The L7007 live/dead bacterial viability kit is used to evaluate the bacteria viability on the anode. The anode with biofilm after MFC test is rinsed with PBS and stained with SYTO 9 dye and propidium iodide (PI) mix solution. The stained cells are examined using a Leica TCS SP8 II confocal/multiphoton laser scanning microscope (Germany). The alive-dead assay solution is prepared by diluting SYTO 9 dye solution (1.67 mM solution in dimethyl sulfoxide) and propidium iodide (1.67 mM solution in dimethyl sulfoxide) stock solutions in PBS at final concentrations of

30 μM and 30 μM. In living bacteria, the SYTO 9 dye will emit strong green fluorescence. In dead bacteria, the PI will bound to DNA and emit red fluorescence.

Coulombic efficiency (QE) and turn-over frequency (TOFs) calculations

The Coulombic efficiency is evaluated by the following equations S1-S3[14]. In equation S1, the η is the Coulombic efficiency, C_{output} is the amount of experimental electric quantity in the microbial fuel cell, in Coulombs. In equation S2, t is the total time in seconds. In equation S3, C_{total} is the total theoretical amount of charge (Q, in Coulombs) transferred in the lactate oxidation process. $C_{lactate}$ is the lactate concentration of the bacteria buffer medium. $V_{solution}$ is the total volume of the medium. n: The number of electrons transferred during the oxidation of one molecule of lactate. F is Faraday's constant (96,500 C/mol).

$$\eta = C_{output}/C_{total} \quad \text{(S1)}$$

$$C_{output} = \int (I \cdot t) \quad \text{(S2)}$$

$$C_{total} = C_{lactate} \cdot V_{solution} \cdot n \cdot F \quad \text{(S3)}$$

The turnover frequency of single bacteria is evaluated using equation S4. Here, $n_{substrate}$ is the total number of lactate molecules that have been oxidized, and t is the total time in seconds. $n_{catalyst}$ is the number of catalysts (and also the bacteria number).

$$\text{Turn-over frequency} = n_{substrate}/t \cdot n_{catalyst} \quad \text{(S4)}$$

3.3 Results and discussions

To fabricate a functional MFC, the bacteria must form the dense biofilms on the anode electrode surface to ensure efficient charge transfer from the individual bacteria to the external

electrode [2], which is the origin of the MFC current and power output [33]. To evaluate the effectiveness of our approach, we have used three different anodic electrode materials: carbon paper, carbon paper with rGO, and carbon paper with rGO/Ag (**Fig. 3.1**) to test the compactness and thickness of the biofilms, in which the carbon paper, the most widely and commercially available MFC anode, and rGO are used for control experiments.

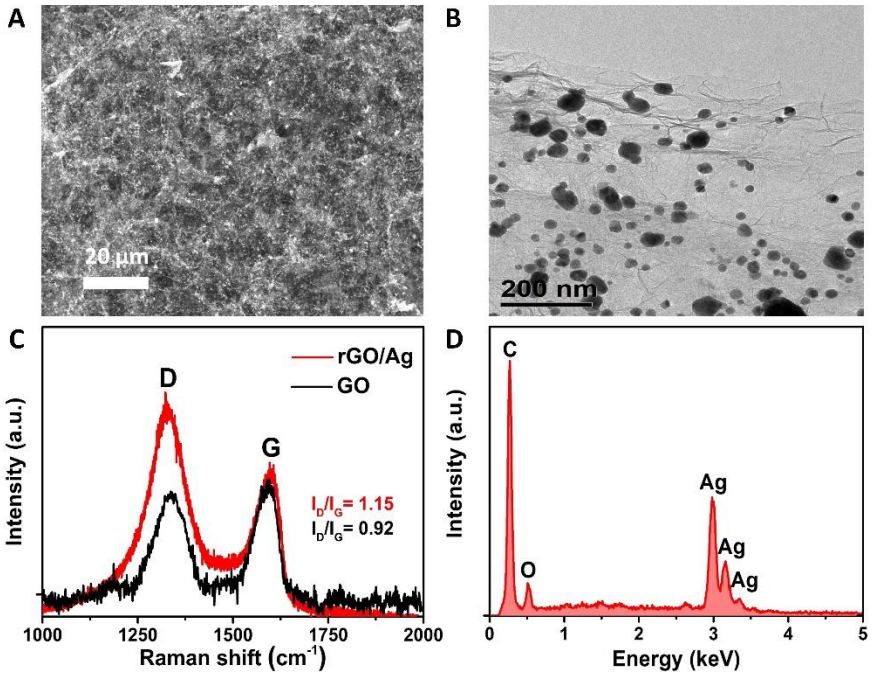

Fig. 3.1. Physical characterization of rGO/Ag. The rGO/Ag anode is synthesized according to the previous report [55]. (**A**) Scanning electron microscope image of rGO/Ag. (**B**) Transmission electron microscope image of rGO/Ag, which shows that the rGO is covered with Ag nanoparticles. The Ag nanoparticles are all attached on the rGO sheets rather than being free-standing. (**C**) Raman spectrum of GO and rGO/Ag, which reveals that the graphene oxide (GO) is reduced with higher I_D/I_G ratio. (**D**) EDS analysis of rGO/Ag (a.u., arbitrary units).

Since Ag is often perceivecd to exhibit antibacterial properties [34], we have first evaluated the biocompatibility of the rGO/Ag electrode and other electrodes with bacteria alive-dead stained assay under the confocal laser scanning microscopy (CLSM). The green fluorescence, which

originates from the SYTO 9 dye in the living bacteria, indicates the rGO/Ag electrode is highly biocompatible (**Fig. 1I, J**). The number of living cells on the rGO/Ag is observed to be much larger than that on the carbon paper (**Fig. 1A, B**) and the carbon paper rGO composite (**Fig. 1E, F**). The quantification shows that the existence of Ag does not undermine the bacterial viability (viability of 93% for rGO/Ag vs. 95% for carbon paper and 92% for rGO, see **Fig. 3.2** for more details).

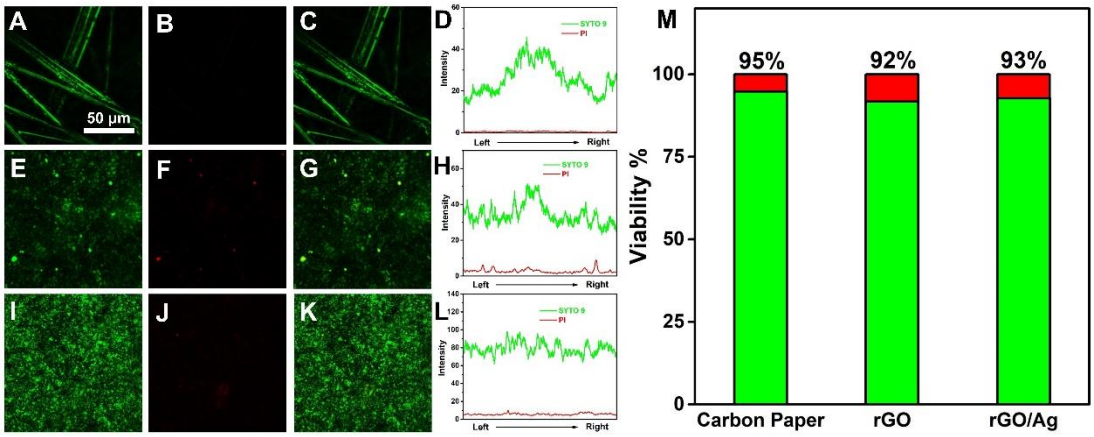

Fig. 3.2. Viability tests based on live/dead kit and confocal laser scanning microscopy (CLSM). The combination of fluorescence dye SYTO 9/propidium iodide (PI) can differentiate live/dead cell under CLSM. Under CLSM images, we observe that on all three electrodes, the green fluorescence intensity is much stronger than the red fluorescence. (**A-C**) Carbon paper biofilm fluorescence of SYTO 9 (green), PI (red) and their overlap; (**D**) Green/red fluorescence intensity comparison; (**E-H**) rGO biofilm green/red fluorescence and intensity; (**I-L**) rGO/Ag biofilm green/red fluorescence and intensity; (**M**) Bacterial viability evaluation determined from the CLSM fluorescence results. These results show that the existence of Ag does not undermine the bacterial viability (rGO/Ag: 93%) compared with the other two electrodes (carbon paper: 95%; rGO: 92%).

Furthermore, scanning electron microscope (SEM) images also reveal distinct biofilm structures with greatly variable bacterial density (SEM, **Fig. 1**). Compact biofilms consisting of densely packed bar-like bacteria (~0.5 μm × ~2 μm) are found on the rGO/Ag electrodes (**Fig. 1K, L**), whereas the biofilms formed on rGO are much less dense (**Fig. 1G, H**), and there are much smaller numbers of bacteria sparsely attached to the carbon fibers of the carbon paper electrodes

(**Fig. 1C, D**). These SEM studies are largely consistent with the confocal fluorescence studies (**Fig. 1A, B, E, F, I, J**). These studies clearly demsontrate the presence of the Ag is beneficial to denser biofilm formation.

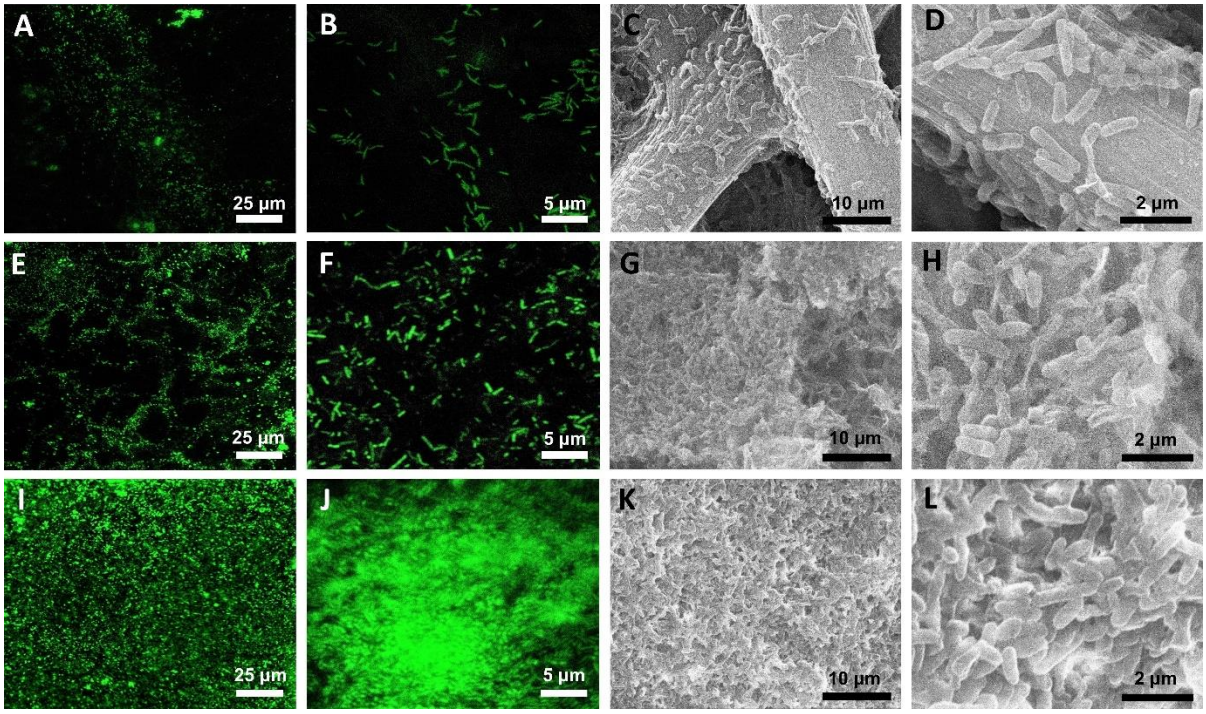

Fig. 3.3. Characterization of *Shewanella* biofilms on three different anodic electrodes: carbon paper, rGO, and rGO/Ag. (**A**, **B**) Confocal laser scanning microscopy (CLSM) images of the *Shewanella* biofilm on the carbon paper. (**C**, **D**) Scanning electron microscope (SEM) images of the biofilm on the carbon paper. (**E**, **F**) CLSM images of biofilm on the rGO. (**G**, **H**) SEM images of biofilm on the rGO. (**I**, **J**) CLSM images of biofilm on the rGO/Ag. (**K**, **L**) SEM images of biofilm on the rGO/Ag.

Excellent cell viability in the presence of Ag may appear counterintuitive because of the strong anti-bacterial function of Ag. We note that the anti-bacterial function of Ag originates from silver ions (Ag^+). For common bacteria *without* exoelectrogenic function, Ag^+ can easily penetrate the bacterial membranes and enter the cell body to combine with the -SH functional group in various of proteins and enzymes and cause their deactivation [34]. Indeed, our own studies with non-exoelectrogenic bacteria, *E. coli*, show that viability decreases to ~50% in the presence of Ag on

the electrode, confirming the antibacterial behavior of Ag to common non-exoelectrogenic bacteria (**Fig. 3.4**). Yet for *Shewanella* and other exoelectrogenic bacteria, a small amount of Ag^{+} can be readily reduced to Ag^{0} by metabolic electrons from various membrane proteins such as MtrABC, which produces transmembrane or outer-membrane Ag nanoparticles and prevents Ag^{+} from entering the cell body and deactivating functional proteins/enzymes, thereby retaining cell viability.

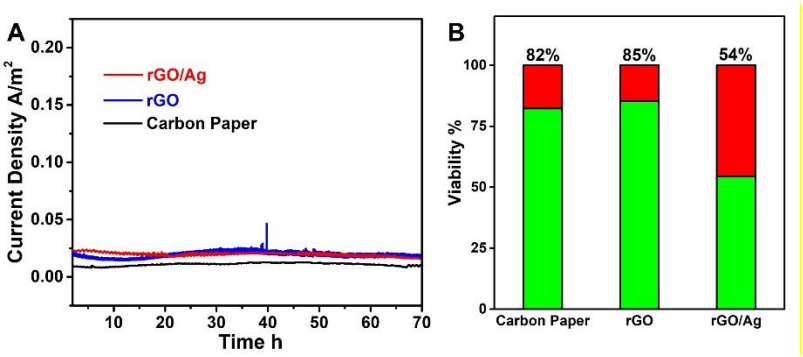

Fig. 3.4. Microbial fuel cell with *E. coli* and viability tests. (**A**) I-t curves of different electrodes with *E. coli*; (**B**) Viability tests of different electrodes after the microbial fuel cell tests in *E. coli*. With the introduction of Ag and antibacterial features, the *E. coli* does not have the ability to reduce the Ag^{+} and the viability is undermined. We found that the viability of *E. coli* decreases from ~80% to ~50% with the presence Ag loading on the electrode.

Before constructing full MFCs, the output current density of the anode materials are first evaluated using three-electrode system electrochemical half-cell MFCs [35]. The carbon paper, rGO and rGO/Ag are each set as the working electrodes, respectively. A positive potential (+0.2 V vs. Ag/AgCl in 1 M KCl solution) is applied on the working electrode [4,36]. The output current density (I) vs. time (t) is recorded as I-t curves (**Fig. 3.5**). The current output of the blank test (with no bacteria added) shows negligible current value throughout the testing period, while the anodic current density of different anodic materials with bacteria show increasing current with time due to the gradual bacteria attachment and biofilm formation. Notably, the maximum current density

output from the rGO/Ag electrode can reach up to 9.2 A/m^2, which is considerably larger than that from either carbon paper (0.6 A/m^2) or rGO (1.2 A/m^2) electrodes.

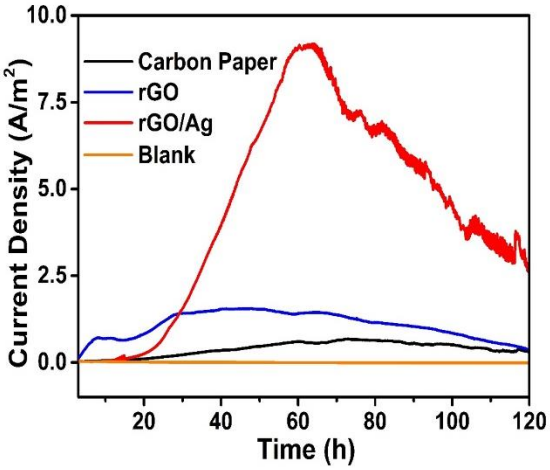

Fig. 3.5. The half-cell MFC tests of different anode electrode as the current vs. time (*I-t*) curves. The maximum current density of different anodic materials follows the order of carbon paper (0.6 A/m^2), rGO (1.2 A/m^2), and rGO/Ag (9.2 A/m^2). The blank test without the bacteria shows negligible current in the entire process.

To test the power output, we have constructed the full MFC in a double chamber container (**Fig. 3.6**) with a 5.5-cm diameter of channel. The carbon paper, rGO and rGO/Ag anodes are positioned in the anodic chamber fed with buffer medium contains 18 mM sodium lactate. The cathode is the carbon cloth (2 cm × 4 cm) coated with 40% Pt/C purged with O_2. The anodic and cathodic chambers are separated with the proton exchange membrane (PEM) Nafion 211. The anode and cathode are connected to a 500 Ω resistor in parallel with a multi-meter to record the output voltage. The output voltage from the MFC increases continuously with incubation time, and reaches a nearly constant value in about 2 days (**Fig. 3.7A**), indicating successful establishment of a functional MFC [14,37].

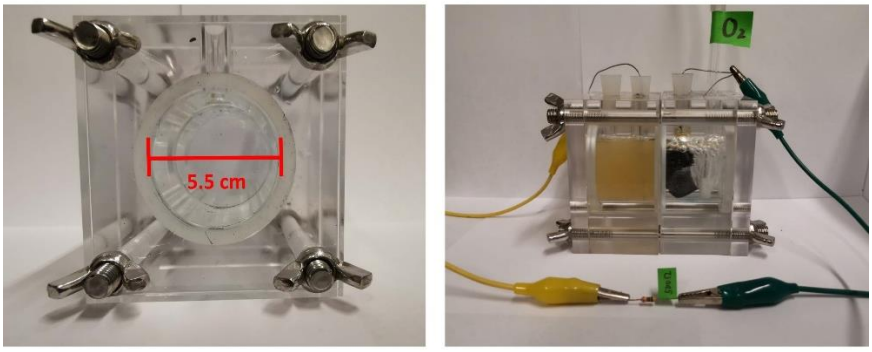

Fig. 3.6. The setup of the double chamber microbial fuel cell (MFC). The H-shaped two-chamber MFC is constructed by connecting two 120 ml chambers with 5.5 cm diameter channels. The cathode is carbon cloth (2 cm × 4 cm) coated with 40% Pt/C with oxygen purging. The anodic solution is purged with ultra-pure nitrogen gas for at least 30 min to remove the dissolved oxygen. The anodic chamber is tightly sealed to maintain anaerobic conditions during MFC operation. All MFC experiments are operated in the static incubator at a temperature of 30 °C.

When the MFC voltage output is steady, different resistors are connected to the anode and the cathode to obtain current vs. voltage (*I-V*) curves and power polarization curves (**Fig. 3.7B**). The *I-V* curves show a similar open circuit voltage around 0.7 V for all three electrodes, consistent with the maximum voltage output from similar MFCs. Notably, the rGO/Ag electrode shows a maximum current output of 38.5 ± 0.5 A/m^2, which is much larger than that from carbon paper (3.4 A/m^2) or rGO (6.2 A/m^2) electrodes, and more than triples the previous record achieved in *Shewanella* MFCs (11 A/m^2) (**Fig. 3.7D**). The maximum power density from the rGO/Ag electrode reaches up to 6.63 ± 0.3 W/m^2, which is also much larger than that for carbon paper anodes (0.51 W/m^2) or rGO anodes (1.34 W/m^2). Such enhancements of power output are highly reproducible and similar results are obtained in repeated tests (**Fig. 3.8**). To the best of our knowledge, the power density achieved with rGO/Ag electrode represents the highest power output from all MFCs reported to date, and more than doubles the highest value reported previously for all *Shewanella*-based MFCs (3 W/m^2) (**Fig. 3.7E**, **Table 1-3**).

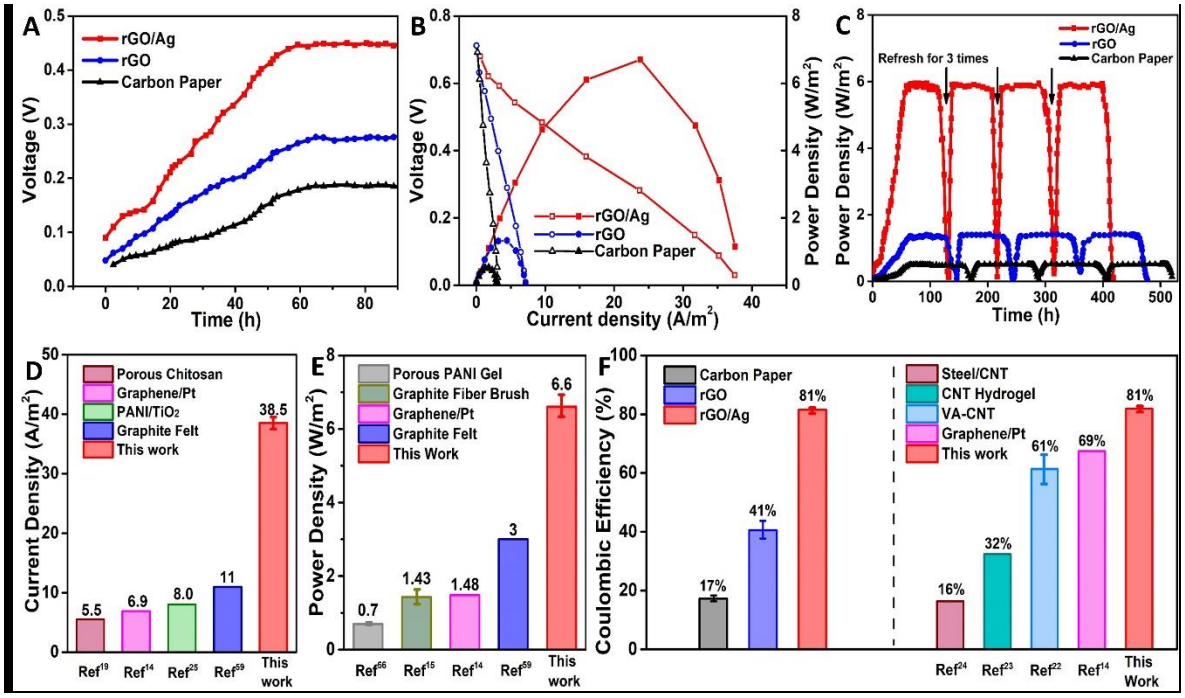

Fig. 3.7. The performance test of *Shewanella* MFCs with different anodes. (**A**) Voltage output of double chamber MFCs with three different anodic materials. (**B**) MFC I-V curves (left axis, open symbols) and power polarization (right axis, filled symbols) curves of three different anodic materials. (**C**) MFC power density vs. time curves for long stability and repeated cycling test. (**D**) The comparison of the current densities with the state-of-art MFCs (PANI: polyaniline). (**E**) The comparison of the MFC power density (PANI: polyaniline). (**F**) Coulombic efficiency (QE) of three different electrodes and their comparison with the state-of-art MFCs (CNT: carbon nanotube, VA: vertical aligned).

Anode (*Shewanella* MR-1)	Current Density A/m^2
Graphene/PANI[21]	5.8
Graphene/Ionic liquid[36]	2.8
Porous PANI gel[56]	3.96
Graphene/CNT[57]	1.2
rGO/Ag (This work)	**9.2**

Table 1. The comparison of the current density of different half-cell MFCs.

Anode	Bacteria	Current Density A/m^2	Power Density W/m^2
Graphite fiber brush[15]	Mix[#]	8.0	1.43
Carbon paper[15]	Mix[#]	2.8	0.5
VA-CNT[22]	*Geobacter*	2.6	0.83
CNT/SnO_2[58]	*E. coli*	3.5	1.42
CNT textile fiber[20]	Mix[#]	5.0	1.1
rGO/Pt[14]	*Shewanella* MR-1	6.9	1.48
3D chitosan hydrogel[19]	*P. aeruginosa*	5.5	1.53
Graphite felt[59]	*Shewanella* DSP10	11	4
rGO/Ag (This work)	***Shewanella* MR-1**	**38.5**	**6.63**

Table 2. The comparison of the current and power density of double chamber MFCs with different anodic materials and bacteria species.[#]The "Mix" means more than two kinds of unspecified bacteria in the system.

Anode	Bacteria	QE
Steel/CNT[#24]	*Geobacter*	16%
CNT Hydrogel[23]	Mix	32%
VA-CNT*[22]	*Geobacter*	61%
rGO/Pt[14]	*Shewanella* MR-1	69%
rGO/Ag (This work)	***Shewanella* MR-1**	**81%**

Table 3. The comparison of the Coulombic efficiency (QE) of MFCs with different anodic materials and bacteria species.[#]"CNT" means carbon nanotube. *"VA" means vertically aligned.

We have also evaluated the output performance of the MFCs over long-term operation. Note that voltage output from the MFC drops sharply after a certain time (~80 h) of stable operation, which could be attributed to the exhaustion of the nutrient in the anode medium. To test this

hypothesis, we have conducted cyclic test by periodically refreshing the anodic medium with nutrient when the voltage output drops below 0.05 V (**Fig. 3.7C**). After adding the new medium with lactate as the nutrient, the output power density is rapidly restored to the original value, which confirms the voltage drop is indeed due to nutrient exhaustion. Similar behavior is observed for all three types of electrodes. Based on the amount of nutrient added and total charge output for each cycle, we can also derive the Coulombic efficiency of the MFCs. Significantly, the MFC with rGO/Ag anode shows a high Coulombic efficiency of ~81%, which is much higher than those with carbon paper (~17%) and rGO (~41%) anodes (**Fig. 3.7F**). We note that the Coulombic efficiency achieved in the MFCs with rGO/Ag anode is also higher than the previous record achieved in *Shewanella* or other MFCs (69%), indicating more efficient utilization of the nutrients for power generation.

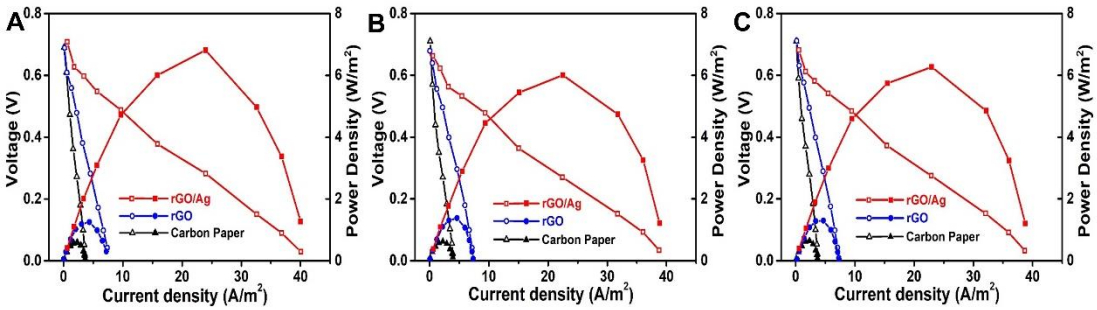

Fig. 3.8. Multi-test of microbial fuel cells show power output ranges from 6.0 W/m^2 to 6.8 W/m^2.

The increased current density from the rGO/Ag anode could possibly be attributed to the higher bacteria density and larger number of bacteria in the anode biofilm, or the more efficient charge transport and less charge loss due to the improved charge transfer process. To decouple these possible contributing factors, we have quantified and compared the number of bacteria in each type of anode by combining the hemocytometer and total nitrogen analysis kit (**Fig. 3.9**).

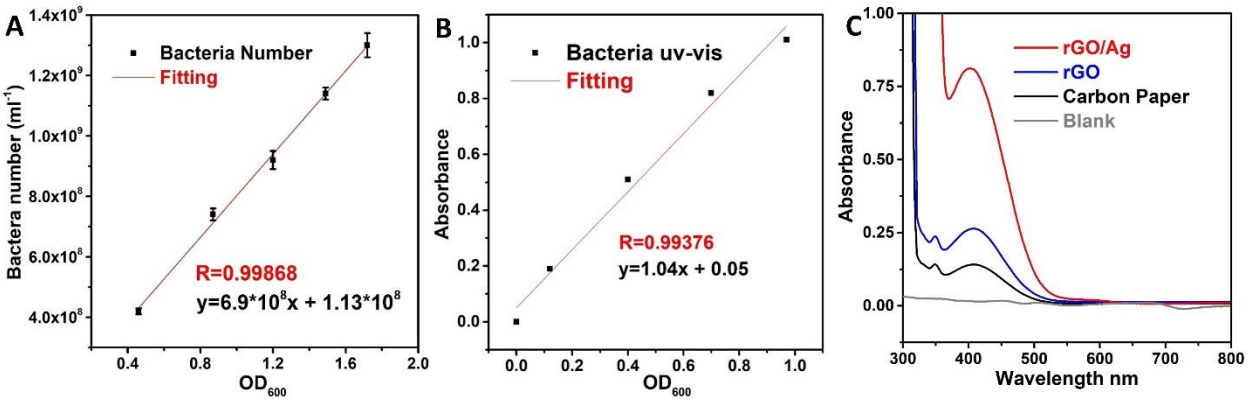

Fig. 3.9. The characterization of bacteria numbers on different electrodes. (**A**) The OD_{600}-Bacteria number standard deviation line based on hemocytometer counting method. (**B**) The OD_{600}-Absorbance standard deviation line based on total nitrogen analysis. (**C**) The absorbance of different number of bacteria on different electrode in the total nitrogen analysis. The testing solution is diluted 3.3 times from the original electrode bacteria solution.

The ratio of bacteria number for the carbon paper, rGO, and rGO/Ag electrodes is 1.0:1.7:5.2 (**Fig. 3.10A**), whereas the MFC current output ratio of the three electrodes is 1.0:1.8:11.3 (**Fig. 3.7B, 3.10B**). With the estimated bacteria number for each electrode and the maximum current output, we can also calculate the turn-over frequency (TOF) for the bacteria on each electrode (**Fig. 3.10C**).

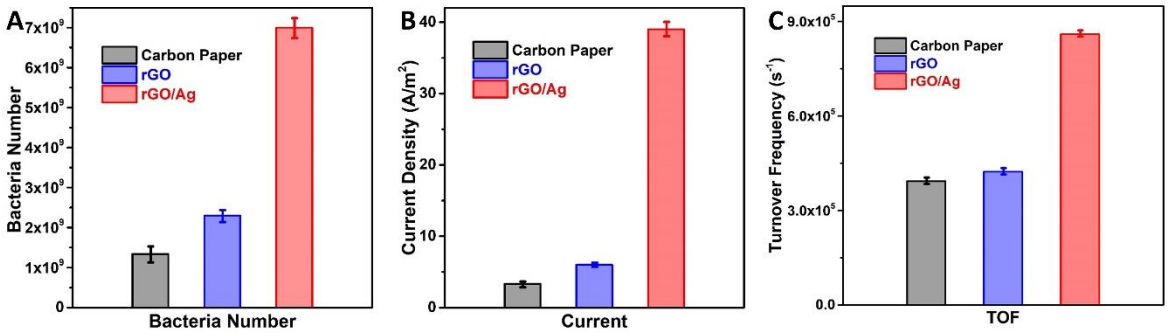

Fig. 3.10. The turnover frequency of *Shewanella* MFCs with different anodes. (**A**) The comparison of bacteria number on three different electrodes. (**B**) The comparison of the maximum current density from three different electrodes. (**C**) The comparison of the calculated turn-over frequency (TOFs) for the biofilm on the carbon paper, rGO and rGO/Ag electrodes.

Note that the bacteria number for the rGO electrode is ~1.7 times that for the carbon paper electrode, and the maximum current obtained from rGO electrode is ~1.8 times that for the carbon paper electrode, suggesting the increased current for the rGO electrode can be largely attributed to the increased bacteria number. Indeed, these two electrodes show a nearly comparable TOF (~3.9×10^5 s^{-1} for carbon paper and ~4.2×10^5 s^{-1} for rGO) (**Fig. 3.11C**), indicating similar charge extraction and transport efficiencies from each bacterium in these two types of electrodes. These TOFs also compare well and slightly favorably with those reported previously (1.6-3.2×10^5 s^{-1}) [38,39]. For the rGO/Ag electrode, the bacteria number is about 5.2 times that of the carbon paper electrode, indicating even denser biofilm formation. Notably, the current output from the rGO/Ag electrode is ~11.3 times of that from the carbon paper electrode. This further increased current output leads to much higher TOFs of ~8.6×10^5 s^{-1} in rGO/Ag electrodes (**Fig. 3.10C**), which is more than double of those for the carbon paper or rGO electrodes. These analyses demonstrate the electron extraction and transport efficiency in the rGO/Ag electrode are much higher than those for the carbon paper or rGO electrodes.

We have expanded our rGO/Ag electrode measurement to various *Shewanella* knock-out mutants: including ΔfccA/ΔSTC/ΔCymA and ΔMtrC/ΔOmcA. Although notable enhancements of the output current or power are also observed with these mutants when Ag is introduced in the rGO scaffold (**Fig. 3.11**, **Table 4**), the overall power output in MFCs from these mutants is lower than those for the wild types.

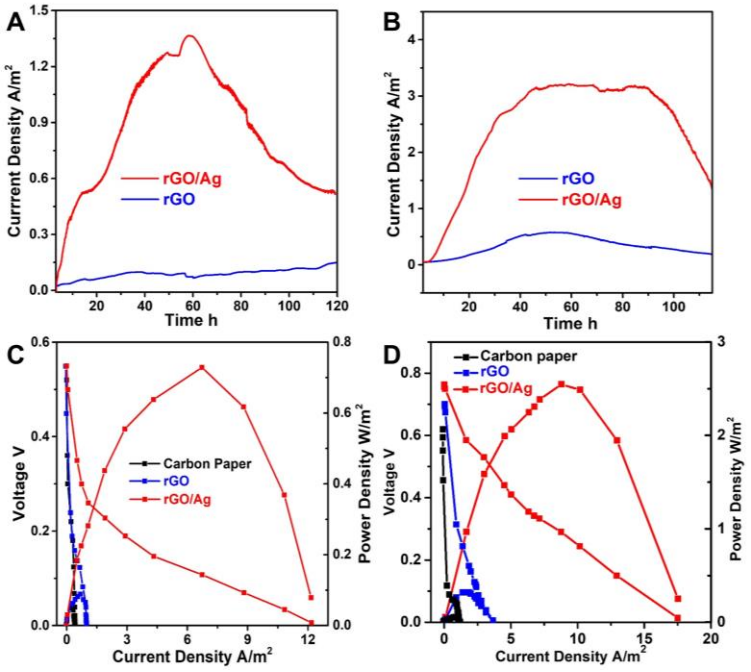

Fig. 3.11. Microbial fuel cell with *Shewanella* mutants ΔfccA/ΔSTC/ΔCymA and ΔMtrC/ΔOmcA. (**A**) I-t curves of different electrodes with ΔfccA/ΔSTC/ΔCymA; (**B**) I-t curves of different electrodes with ΔMtrC/ΔOmcA; (**C**) Microbial fuel cell full cell performance tests of different electrodes with ΔfccA/ΔSTC/ΔCymA; (**D**) Full cell performance tests of different electrodes with ΔMtrC/ΔOmcA**.** These studies suggest that the trans/outer-membrane Ag nanoparticle can enhance the transmembrane and extracellular electron transport for all types cells including wild types and various knockouts, but cannot completely make up the performance lost for knockouts.

These results are not surprising considering that the trans/outer-membrane Ag nanoparticles are produced from reduction of Ag^{+} by metabolic electrons and the loss of membrane proteins in these different mutants can limit the transport of metabolic electrons and partly suppress the formation of trans/outer-membrane Ag nanoparticles. Additionally, we have tested non-exoelectrogenic bacteria, such as *E. coli*, and did not see significant current output with either rGO or rGO/Ag electrodes (**Fig. 3.4**).

	Wild Type	ΔfccA/ΔSTC/ΔCymA	ΔMtrC/ΔOmcA

rGO	6.2 A/m^2/1.34 W/m^2	0.9 A/m^2/0.09 W/m^2	3.9 A/m^2/0.48 W/m^2
rGO/Ag	38.5 A/m^2/6.63 W/m^2	12.1 A/m^2/0.71 W/m^2	17.5 A/m^2/2.52 W/m^2

Table 4.MFC performance comparison of *Shewenalla* wild type and 2 other mutants, ΔfccA/ΔSTC/ΔCymA and ΔMtrC/ΔOmcA.

Although previous studies have suggested that the inclusion of noble metal nanoparticles and semiconductor nanoparticles on the rGO sheets could help reduce the electrode charge transfer resistance (R_{ct}) [25,26], such a decrease in R_{ct} cannot readily explain the performance differences among the three different electrodes. Specifically, our electrochemical impedance spectroscopy (EIS) measurements of the electrodes without bacteria show that carbon paper exhibits a much larger R_{ct} of 95 Ω, while the rGO and rGO/Ag electrode exhibit a rather similar R_{ct} of 49 Ω and 40 Ω (**Fig. 3.12**), respectively, which cannot explain the much higher TOFs observed in rGO/Ag electrodes than those in carbon paper or rGO electrodes. Moreover, the resistance of the electrode scaffold should not significantly influence the TOF, which should be an intrinsic feature of the bacterial metabolism and charge extraction efficiency.

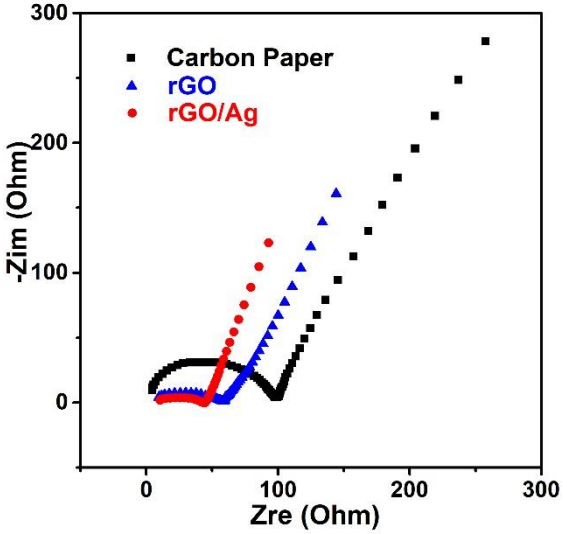

Fig. 3.12. Electrochemical impedance spectroscopy (EIS) Nyquist curves of carbon paper, rGO and rGO/Ag and the zoom-in image. The carbon paper exhibits a much larger R_{ct} of 95 Ω, while the rGO and rGO/Ag electrode exhibit a rather similar R_{ct} of 49 Ω and 40 Ω. The lower R_{ct} in rGO or rGO/Ag than that of carbon paper is attributed to more hydrophilic surfaces and better wettability of rGO or rGO/Ag than carbon paper.

Our electrochemical surface area (ECSA) studies show that the introduction of rGO on carbon paper can considerably increase the total surface area, by ~14 times, while the introduction of Ag only results in a relatively small additional increase (~20%), which cannot account for the much-improved performance for rGO/Ag electrodes (vs. rGO electrodes, **Fig. 3.13**).

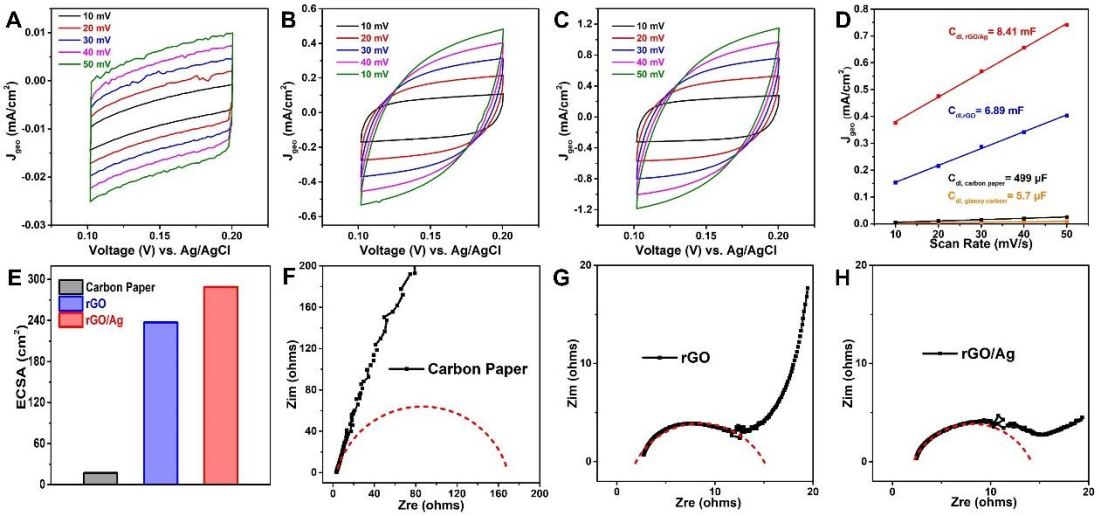

Fig. 3.13.C_{dl} and corresponding ECSAs of the three different electrodes. (**A-C**) CV curves of the carbon paper, rGO and rGO/Ag electrode in the non-faradic range in the medium buffer solution; (**D**) C_{dl} results of the various electrodes obtained from CV; (**E**) ECSA values of the various electrodes: carbon paper: 17 cm^2; rGO: 235 cm^2; rGO/Ag: 284 cm^2. (**F-H**) EIS tests of different electrodes in the medium buffer solution. the difference in ECSA for three different electrodes matches well with (and accounts for) different ion absorption R_{ct} values determined for carbon paper (~166 Ω), rGO (14 Ω), and rGO/Ag (12 Ω) in the medium buffer solution.

Besides, we have conducted preliminary omics analyses. Considering that the electrons originate from lactate dehydrogenation to NADH, followed by quinone/quinol redox reactions,

and a series of membrane proteins, we have analyzed the related proteins omics results (**Table 5**) In general, for *Shewanella* with and without the Ag, we see no apparent differences in proteins related to EET metabolism or membrane proteins.

Protein Name	Protein Function	Amount (no Ag^+)	Amount (with Ag^+)
L-lactate dehydrogenase complex protein (LldE)	Lactate oxidation	0.108%	0.136%
L-lactate dehydrogenase iron-sulfur cluster-binding protein (LldF)		0.362%	0.393%
Respiratory FAD-dependent D-lactate dehydrogenase (Dld)		0.340%	0.377%
L-lactate dehydrogenase complex protein (LldG)		0.094%	0.117%
NADH-quinone oxidoreductase subunit B, C/D, E, F, G, H, I, J, L, M, N	Electron transfer from NADH to quinone	0.326%	0.340%
Ubiquinol-cytochrome c reductase iron-sulfur subunit	Electron transfer from quinol to CymA	0.086%	0.074%
CymA	Inner membrane electron transfer	0.046%	0.056%
FccA	Transmembrane electron transfer	0.304%	0.343%
MtrA/B/C	Outer membrane electron transfer	0.038%/0.318%/0.218%	0.043%/0.246%/0.206%

OmcA		0.332%	0.294%

Table 5. Proteomics analyses of proteins related electron transfer process.

To elucidate the origin of the enhanced charge extraction efficiency and the boosted TOFs in rGO/Ag electrode, we have conducted scanning transmission electron microscopy (STEM) and energy-dispersive X-ray spectroscopy (EDX) elemental mapping of the bacteria on the rGO/Ag anode after a complete MFC cycle. The STEM and EDX mapping studies indicate enrichment of Ag around the *Shewanella* (**Fig. 3.14A**). To evaluate the spatial distribution Ag within individual bacterium, we have conducted the STEM image and EDX elemental mapping studies on ultrathin sections of *Shewanella*-Ag hybrids. Notably, we found abundant Ag nanoparticles near, inside, and across the membrane area of the *Shewanella* cells (**Fig. 3.14B**). The formation of Ag nanoparticles near the membrane area is not surprising considering the heavy metal tolerance of *Shewanella* and the well-known metal reduction capability of these types of bacteria [4,10]. In this case, a likely scenario is that the rGO/Ag electrode slowly releases the silver ions, which diffuse toward *Shewanella* and are reduced *in situ* by the metabolic electrons generated in *Shewanella* to form Ag nanoparticles on and in the cytoplasmic membranes.

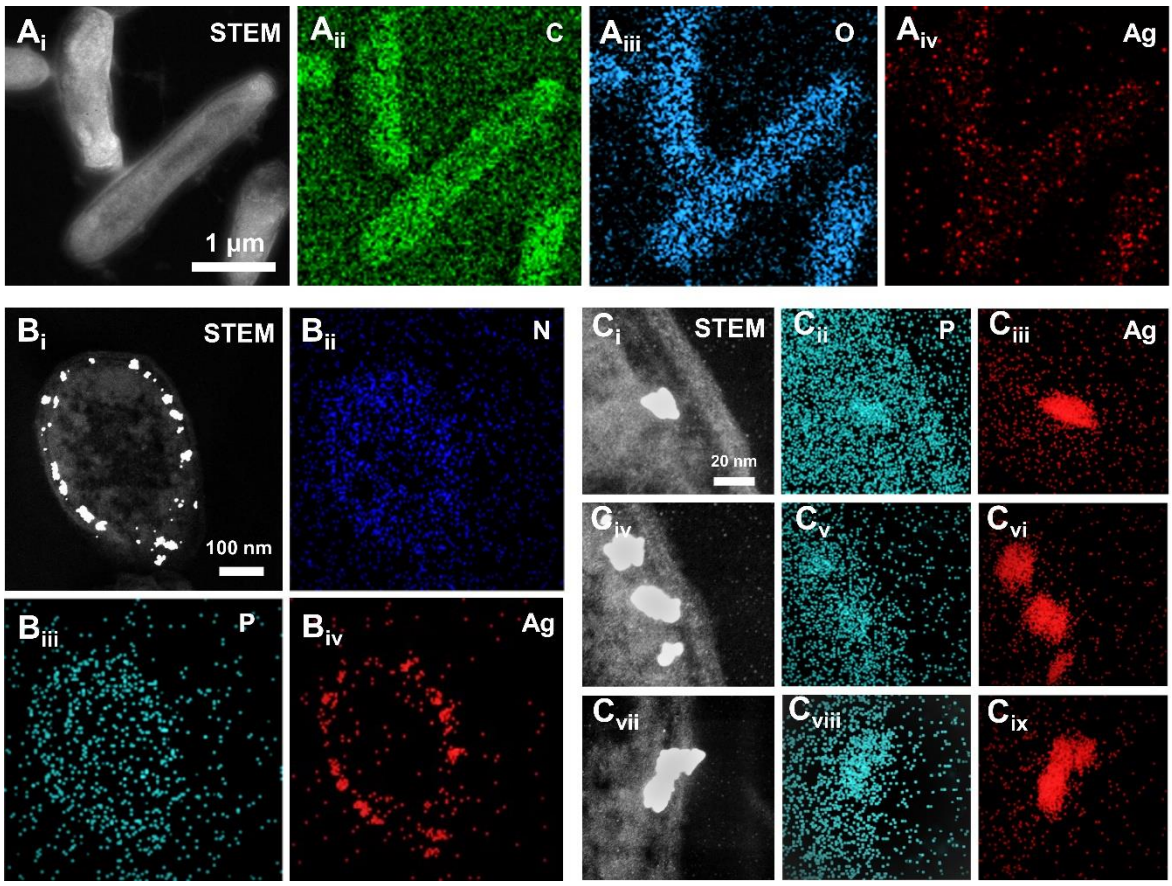

Fig. 3.14. Characterization of single bacterium and transmembrane structure. (**A**) Scanning transmission electron microscopy (STEM) image and energy-dispersive X-ray spectroscopy (EDX) elemental (carbon, oxygen and silver) mapping of the bacteria on the rGO/Ag electrode. (**B**) STEM image and EDX mapping of the ultrathin sections of the bacteria on the rGO/Ag electrode. (**C**) STEM image and EDX elemental mapping of the transmembrane silver nanoparticles inside and traversing the cell membranes.

Notably, high-reolution STEM images and and the corresponding EDX mapping images clearly show some Ag nanoparticles traverse the entire periplasmic space between the inner and outer membranes and break through the outer membrane (**Fig. 3.14C**). In the membrane cytochromes involved in transmembrane and extracellular electron transfer processes, electrons are transferred through multistep hopping between the Fe^{3+}/Fe^{2+} redox centers [40]. Since the metal electronic conductivity is far higher than the redox-center-mediated transfer in cytochromes

(membrane or nanowires) [41,42], the transmembrane and outer-membrane Ag nanoparticles can act as metallic shortcuts to bypass the sluggish electron transfer process mediated by the redox centers, making direct contacts with external electrodes for more efficient charge extraction.

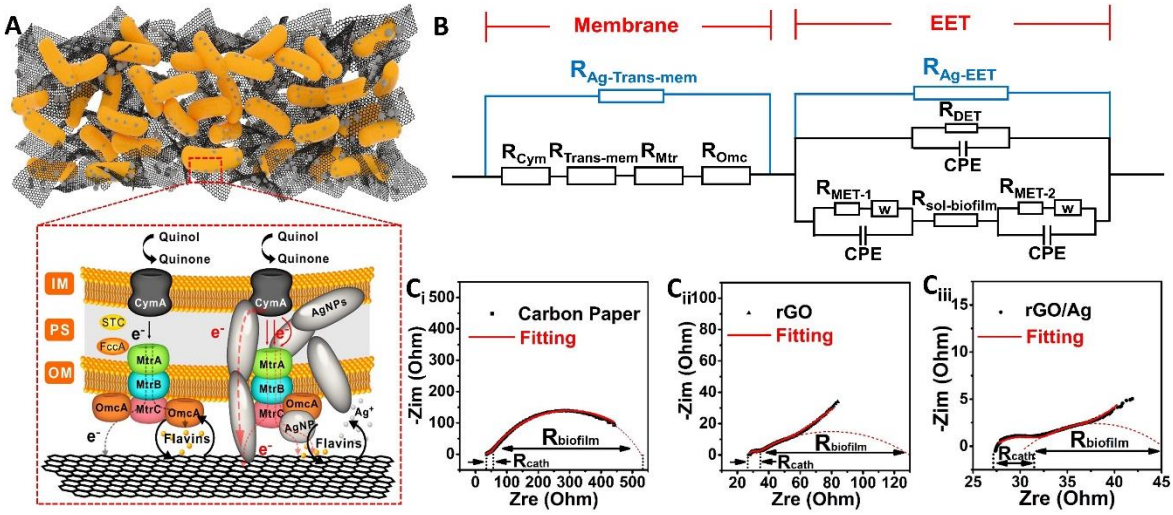

Fig. 3.15. Schematic illustration of biofilm on rGO/Ag anode and electrochemical impedance spectra (EIS) tests. (**A**) The rGO/Ag anode releases the Ag^+ ions that help *Shewanella* biofilm formation and *in situ* production of trans/outer-membrane Ag nanoparticles in *Shewanella*. In the *Shewanella*-Ag hybrids, the Ag nanoparticles can provide additional metallic pathways to facilitate the transmembrane and extracellular electron transfer processes. Some Ag nanoparticles can also provide direct electron pathways from the inner membrane to the electrode. (**B**) The equivalent circuit of transmembrane and extracellular electron transfer processes. The $R_{sol\text{-}biofilm}$ is the resistance when mediators going through the biofilm solutions between the bacteria and electrode. The $R_{MET\text{-}1}$ is the charge transfer resistance of flavin reduction cycle at the bacteria and the $R_{MET\text{-}2}$ is charge transfer resistance of the flavin oxidation cycle at the electrode. The $R_{Ag\text{-}Trans\text{-}mem}$ is the resistance when the electron flux is through transmembrane Ag nanoparticles rather than cytochrome redox centers. The $R_{Ag\text{-}EET}$ is from *in situ* Ag nanoparticles breaking through the outer membranes and directly contacting the electrode. (**C**) The electrochemical impedance spectra (EIS) of the biofilms on different electrodes (carbon paper, rGO and rGO/Ag) along with the fitting curves. The R_{cath} is the charge transfer resistance of ferricyanide cathode reactions. The $R_{biofilm}$ is the charge transfer resistance from the anode bacteria biofilm.

The benefit of the Ag nanoparticles in the transmembrane and extracellular electron transfer processes (**Fig. 3.15A**) can be further illustrated by constructing the equivalent circuit (Fig. 3.15B).

Without Ag nanoparticle, the metabolic electrons in the cytoplasm are first transferred through the CymA on the inner membrane [43,44] from which they cross the periplasm by hopping from the CymA cytochromes redox centers to the periplasmic c-Cyts FccA and small tetrahaem cytochrome (STC) [45,46] (**Fig. 3.15A**), as represented in R_{Cym} and $R_{Trans\text{-}mem}$ in the equivalent circuits (**Fig. 3.15B**). On the outer membrane, the electrons are transferred via membrane proteins MtrA, MtrB, MtrC, and OmcA (R_{Mtr} and R_{Omc}) to the electrode surface through extracellular electron transfer (EET) process that includes two parallel paths: across proteins MtrC and OmcA to the electrode via direct electrical contact as represented by direct electron transfer resistance (R_{DET}), and indirect redox shuttling process mediated by the bacteria secreted flavins as represented by mediated electron transfer resistance (R_{MET}) [47,48]. The Ag nanoparticles embedded within and across the membrane provide additional metallic transport pathways, which contribute to transmembrane electron transfer, increasing the electron flux from the metabolic process for the subsequent extracellular electron transfer process to the electrode, and also directly contribute to more efficient extracellular electron transfer process through direct electrical contact with electrode surface. Both effects lead to more efficient charge extraction, higher TOF values and MFC output performance.

To probe the contributions of Ag nanoparticles in the charge transfer process, we have further conducted electrochemical impedance spectroscopy (EIS) studies on all three type of MFCs consisting of bacteria biofilm anodes made on carbon paper, rGO, and rGO/Ag (**Fig. 3.16C**). The Nyquist plots show two semicircles that can be attributed to the charge transfer processes in cathode and anode (see **Fig. 3.16** for the equivalent circuit).

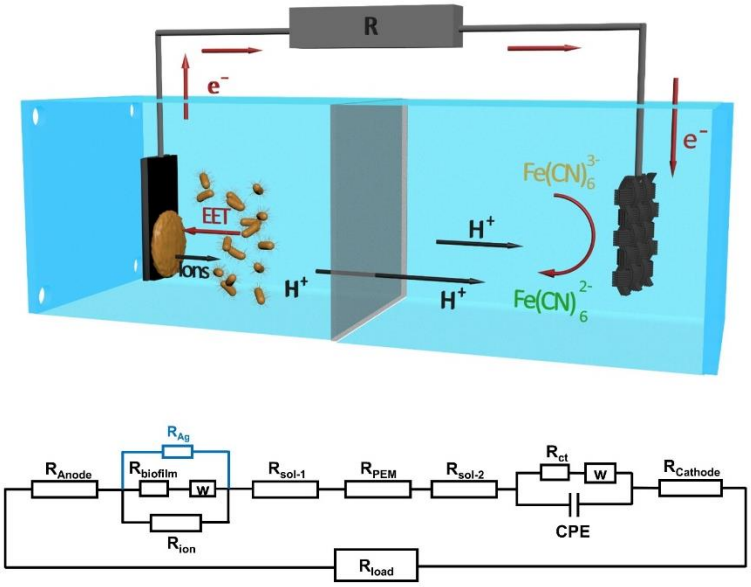

Fig. 3.16. The equivalent circuit of the double chambers microbial fuel cell (MFC). The R_{anode} and $R_{cathode}$ represent the Ohmic resistance of anode and cathode resistance. The R_{sol} and R_{PEM} are the solution resistance and proton exchange membrane resistance. The $R_{biofilm}$ corresponds to the *Shewanella* biofilm extracellular electron transfer (EET). The R_{ion} is related to the ion transfer across the *Shewanella* biofilm. The R_{ct} is the charge transfer resistance of the cathode reaction.

The first semicircle for all three types of device gives a comparable charge transfer resistance of ~7 Ω, which represents the contribution from the cathode reaction and is largely independent from the anode reaction, as also identified by the same semicircles shown in the MFC blank tests (**Fig. 3.17**).

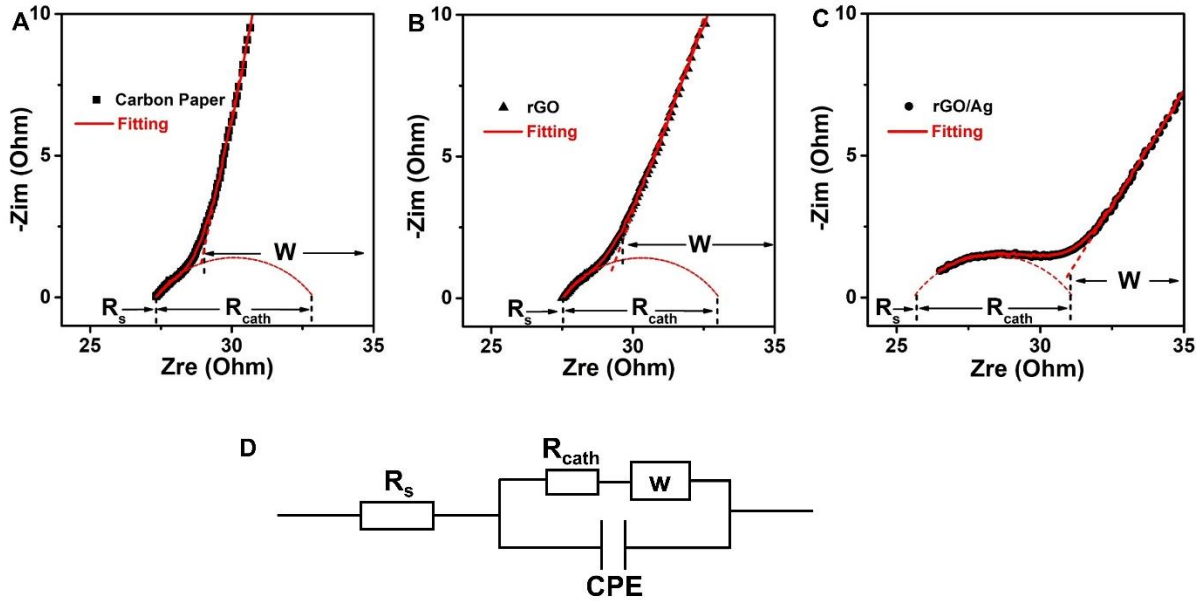

Fig. 3.17. The EIS tests of MFC blank tests. In the blank control tests (**A-C**), the setup is the same as for the MFC tests except no bacteria are added in the anodic chamber. The system is dictated by the cathode reaction as illustrated in the equivalent circuit diagram (**D**). The red solid lines are the best fitting line for each EIS data. The R_s is the sum of the MFC Ohmic resistance. The R_{cath} represents the value of cathode ferricyanide reduction reaction. The values of R_s and R_{cath} are listed in Table 6.

The second semicircle originates from the *Shewanella* biofilm and gives highly distinct charge transfer resistance values ($R_{biofilm}$) of 482 Ω, 102 Ω, and 16 Ω for the anodes with carbon paper, rGO, and rGO/Ag, respectively. Since the Ag nanoparticles in the biofilm network can provide alternative charge transport pathways with much smaller resistances, the charge transfer resistance of the biofilm with embedded Ag nanoparticles are greatly reduced, which can be attributed to the increased bacteria numbers and more importantly, the improved transmembrane and extracellular electron transfer efficiency due to the Ag nanoparticle shortcuts. In particular, the improved TOFs in rGO/Ag electrode is largely attributed to the increased electron transfer efficiency.

Blank	carbon paper	rGO	rGO/Ag

R_s	27.2	27.6	26.3
R_{cath}	6.2	5.8	5.9

MFC	carbon paper	rGO	rGO/Ag
R_s	36.5	27.6	27.0
R_{cath}	6.8	6.9	6.8
$R_{biofilm}$	482	102	16

Table 6. The resistance value determined from the blank and MFC EIS tests. The anodic electrodes are carbon paper, rGO and rGO/Ag.

To further prove the positive effect of Ag and the TOF enhancement on single cell level, we have designed an on-chip microbial fuel cell test with a flat metal (Au) electrode that enables us to monitor the surface bacterium density actively, during the fuel cell test. Our on-chip studies also show a similar nearly two times enhancement in TOF in the sub-monolayer bacterium density when Ag is introduced into the system. Note that inter-cellular charge transfer plays little role in such on-chip devices with sub-monolayer bacterium density since each bacterium is in direct contact with the electrode surface. We also note that although such on-chip studies further confirm the enhancement effect by Ag and largely exclude the inter-cellular transport contribution, they do not exclude the contribution of extracellular electron transport or across cell/electrode interface, and we believe such contributions could indeed enhance charge transport in the MFCs as well.

For the on-chip electrode, the Ti/Au electrode is fabricated through photolithography and electron-beam lithography with the scale of 500 μm × 500 μm (**Fig. 3.18A**). The entire sample surface is covered with PMMA except the electrode area, where there is a window opened to expose the metal electrode to the *Shewanella* bacterium suspension as the working electrode. To

introduce Ag into the system, an Ag layer is coated on top of the Ti/Au to obtain Ti/Au/Ag electrode (**Fig. 3.18B**). During the microbial fuel cell test, we applied a positive voltage (+200 mV) to the working electrode to attract bacteria for further loading and extracellular electron transfer (EET). The surface density of the bacteria is monitored with optical microscopy at different testing times. The current vs. time (I-t) tests show that the output current density of Ti/Au/Ag (0.082 A/m^2) is notably higher than the Ti/Au electrode (0.045 A/m^2, **Fig. 3.18C**). This result further confirms the enhancement effect of the coated silver. The microscopic images of the electrode surface show the bacterial density on the electrode increases with increasing testing time (**Fig. 3.18D**, **3.18E**). The bacterium number is counted under the microscope for the first 16 h, which allows us to determine the TOF value of ~5.2×10^5 s^{-1} and ~3.1×10^5 s^{-1} for electrodes with and without the Ag coating. These results are comparable to our results obtained from carbon-paper/rGO/Ag electrodes

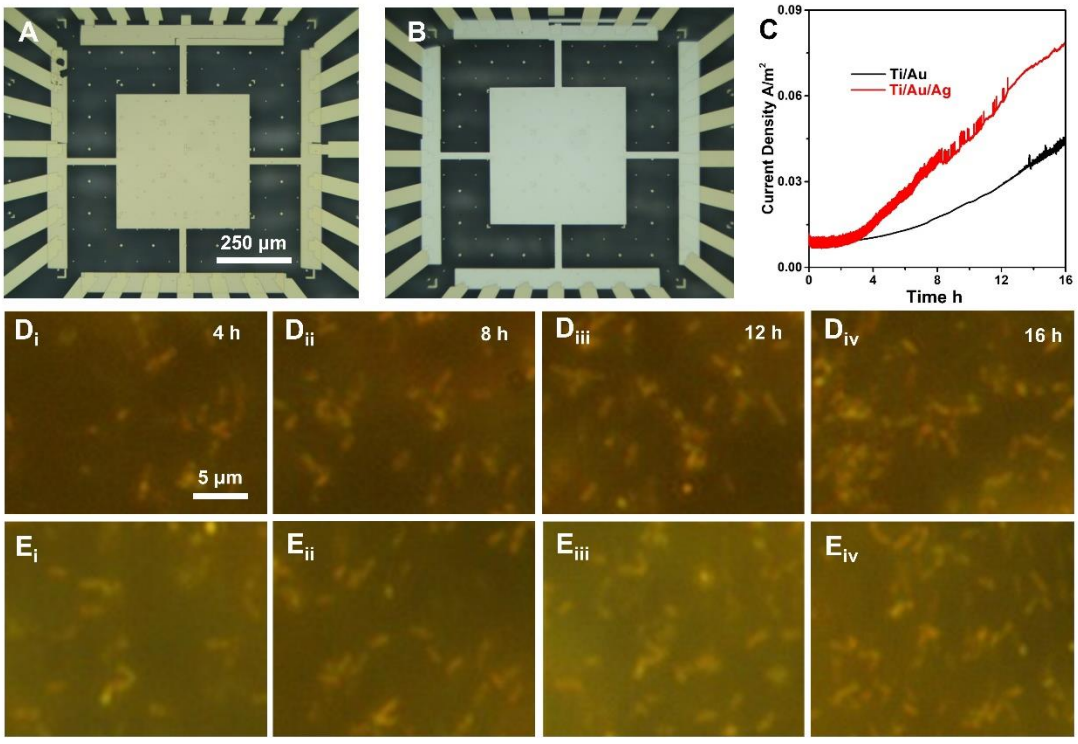

Fig. 3.18. On-chip microbial fuel cell tests that directly correlate the current output vs. cell number. (**A, B**) Pristine 500 μm × 500 μm Ti/Au electrodes and pristine 500 μm × 500 μm

Ti/Au/Ag; (**C**) Output current density of the metal electrodes with (red) and without Ag coverage (black); (**D**) *Shewanella* density increases on Ti/Au electrode at testing times: 4h, 8h, 12h, and 16h; (**E**) *Shewanella* density increases on Ti/Au/Ag at testing times: 4h, 8h, 12h, and 16h.

To this end, we have conducted additional experiments with rGO electrodes (without pre-formed Ag nanoparticles). By using a syringe pump to add a small amount of Ag ion solution gradually to the experimental system while collecting the I-t curves (**Fig. 3.19**), we achieved similar enhancements of the current output, suggesting the metabolic reduction of Ag ions to form trans/outer-membrane Ag nanoparticles (instead of Ag nanoparticles loaded on the rGO/Ag) are primarily responsible for the improved current output.

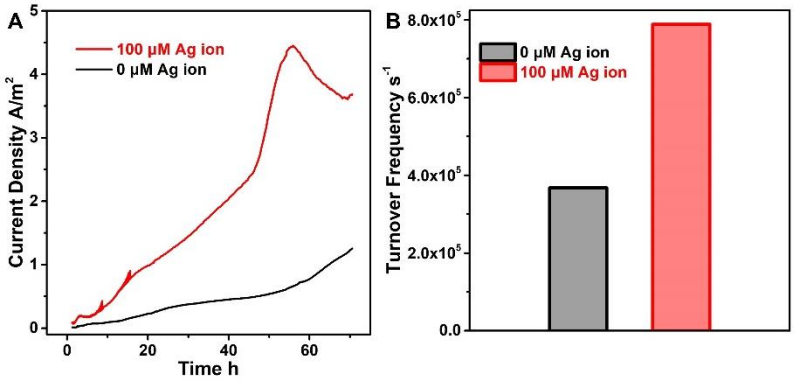

Fig. 3.19. The I-t measurements of rGO electrodes with Ag ion solution and TOF calculations. (**A**) I-t curves of a rGO electrode with pristine bacteria (black) and with Ag ions added (red). 3 ml of Ag ion solution (1 mM) is added at constant speed during the testing time by syringe pump, resulting in a final concentration Ag of 100 μM. (**B**) The TOFs of the rGO electrode with pristine *Shewanella* and additional Ag ions. Adding Ag ion solution can also make the TOFs double during the I-t tests.

Under anaerobic conditions with the lactate as the solitary nutrient, the electrons transferred extracellularly mostly originate from the lactate dehydrogenation process facilitated by lactate dehydrogenase (LDH) [49]. It is therefore interesting to compare the TOFs achieved in our *Shewanella* biofilm with those achieved in individual enzyme or in inorganic catalysts for similar

reactions. Considering that the approximate copies of LDH in a bacterium is ~1,000 [50,51], the TOFs estimated for single LDH are 394 s^{-1} for normal *Shewanella* and 860 s^{-1} for *Shewanella*-Ag hybrids, which compare favorably with those reported for isolated LDH (TOF ~ 170-300 s^{-1}) [52,53]. In particular, the TOFs achieved in the *Shewanella*-Ag hybrid biofilm are notably higher, confirming the critical roles of the transmembrane Ag nanoparticles in boosting the charge extraction and transfer efficiency. Lastly, we note that the TOFs achieved in LDH in the *Shewanella* biofilms are several orders of magnitude higher than that achieved in lactate dehydrogenation inorganic catalysts (~0.03 s^{-1}) [54], which highlights the obvious merits of these exoelectrogenic bacteria in catalyzing the complex lactate oxidation process for power generation.

Together, we have designed and demonstrated a rGO/Ag anodic electrode for constructing high density *Shewanella* biofilms to enable MFCs with a high current density of 38.5 A/m^2, high power density of 6.63 W/m^2, and Coulombic efficiency of 81%. These values all are the highest reported for MFCs to date. Taking advantage of the heavy metal ion tolerance of *Shewanella*, the silver ions released by the rGO/Ag electrode can be reduced *in situ* by metabolic electrons to produce trans/outer-membrane Ag nanoparticles, which can greatly boost the transmembrane and extracellular electron transfer to produce higher TOF and higher power output. Our study highlights that engineering *Shewanella*-Ag hybrids with transmembrane metallic nanoparticles provides an effective pathway to break the electron transfer limit in typical natural bacteria and to push the limit of the MFCs.

3.4 References

1. Rabaey, K. & Verstraete, W. Microbial fuel cells: Novel biotechnology for energy generation. *Trends Biotechnol.* **23**, 291–298 (2005).

2. Lu, L. *et al.* Wastewater treatment for carbon capture and utilization. *Nat. Sustain.* **1**, 750–758 (2018).

3. Bruce E. Logan. Conversion of wastes into bioelectricity and chemicals by using microbial electrochemical technologies. *Science.* **337**, 686–890 (2012).

4. Logan, B. E. Exoelectrogenic bacteria that power microbial fuel cells. *Nat. Rev. Microbiol.* **7**, 375–381 (2009).

5. Logan, B. E. & Regan, J. M. Electricity-producing bacterial communities in microbial fuel cells. *Trends Microbiol.* **14**, 512–518 (2006).

6. Logan, B. E. *et al.* Microbial fuel cells: Methodology and technology. *Environ. Sci. Technol.* **40**, 5181–5192 (2006).

7. Simonsson, D. Electrochemistry for a cleaner environment. *Chem.Soc.Rev.* **26**, 181–189 (1997).

8. Lovley, D. R. Bug juice: Harvesting electricity with microorganisms. *Nat. Rev. Microbiol.* **4**, 497–508 (2006).

9. Min, B., Kim, J. R., Oh, S. E., Regan, J. M. & Logan, B. E. Electricity generation from swine wastewater using microbial fuel cells. *Water Res.* **39**, 4961–4968 (2005).

10. Logan, B. E., Rossi, R., Ragab, A. & Saikaly, P. E. Electroactive microorganisms in bioelectrochemical systems. *Nature Reviews Microbiology* **17**, 307–319 (2019).

11. Liu, H., Ramnarayanan, R. & Logan, B. E. Production of electricity during wastewater treatment using a single chamber microbial fuel cell. *Environ. Sci. Technol.* **38**, 2281–2285 (2004).

12. Jiang, X. *et al.* Nanoparticle facilitated extracellular electron transfer in microbial fuel cells. *Nano Lett.* **14**, 6737–6742 (2014).

13. Wu, X. *et al.* A role for microbial palladium nanoparticles in extracellular electron transfer. *Angew. Chemie - Int. Ed.* **50**, 427–430 (2011).

14. Zhao, S. *et al.* Energy Resources: Three-dimensional graphene/Pt nanoparticle composites as freestanding anode for enhancing performance of microbial fuel cells. *Sci. Adv.* **1**, 1–9 (2015).

15. Logan, B., Cheng, S., Watson, V. & Estadt, G. Graphite fiber brush anodes for increased power production in air-cathode microbial fuel cells. *Environ. Sci. Technol.* **41**, 3341–3346 (2007).

16. Arends, J. B. A., Blondeel, E., Tennison, S. R., Boon, N. & Verstraete, W. Suitability of granular carbon as an anode material for sediment microbial fuel cells. *J. Soils Sediments* **12**, 1197–1206 (2012).

17. Li, C., Zhang, L., Ding, L., Ren, H. & Cui, H. Effect of conductive polymers coated anode on the performance of microbial fuel cells (MFCs) and its biodiversity analysis. *Biosens. Bioelectron.* **26**, 4169–4176 (2011).

18. Cheng, S. & Logan, B. E. Ammonia treatment of carbon cloth anodes to enhance power generation of microbial fuel cells. *Electrochem. commun.* **9**, 492–496 (2007).

19. He, Z., Liu, J., Qiao, Y., Li, C. M. & Tan, T. T. Y. Architecture engineering of hierarchically porous chitosan/vacuum-stripped graphene scaffold as bioanode for high performance microbial fuel cell. *Nano Lett.* **12**, 4738–4741 (2012).

20. Yuan, Y., Zhou, S., Liu, Y. & Tang, J. Nanostructured macroporous bioanode based on polyaniline-modified natural loofah sponge for high-performance microbial fuel cells. *Environ. Sci. Technol.* **47**, 14525–14532 (2013).

21. Zhao, C. *et al.* Polyaniline networks grown on graphene nanoribbons-coated carbon paper with a synergistic effect for high-performance microbial fuel cells. *J. Mater. Chem. A* **1**, 12587–12594 (2013).

22. Ren, H. *et al.* A high power density miniaturized microbial fuel cell having carbon nanotube anodes. *J. Power Sources* **273**, 823–830 (2015).

23. Liu, X. W. *et al.* Conductive carbon nanotube hydrogel as a bioanode for enhanced microbial electrocatalysis. *ACS Appl. Mater. Interfaces* **6**, 8158–8164 (2014).

24. Zhang, Y., Sun, J., Hu, Y., Li, S. & Xu, Q. Carbon nanotube-coated stainless steel mesh for enhanced oxygen reduction in biocathode microbial fuel cells. *J. Power Sources* **239**, 169–174 (2013).

25. Qiao, Y. *et al.* Nanostructured polyaniline/titanium dioxide composite anode for microbial fuel cells. *ACS Nano* **2**, 113–119 (2008).

26. Wang, R. *et al.* FeS_2 nanoparticles decorated graphene as microbial-fuel-cell anode achieving high power density. *Adv. Mater.* **30**, 1–7 (2018).

27. Bird, L. J., Bonnefoy, V. & Newman, D. K. Bioenergetic challenges of microbial iron metabolisms. *Trends Microbiol.* **19**, 330–340 (2011).

28. Fu, T. *et al.* Bioinspired bio-voltage memristors. *Nat. Commun.* **11**, 1–10 (2020).

29. Ding, M. *et al.* Nanoelectronic Investigation Reveals the Electrochemical Basis of Electrical Conductivity in *Shewanella* and *Geobacter*. *ACS Nano* **10**, 9919–9926 (2016).

30. El-Naggar, M. Y. *et al.* Electrical transport along bacterial nanowires from *Shewanella oneidensis* MR-1. *Proc. Natl. Acad. Sci. U. S. A.* **107**, 18127–18131 (2010).

31. Cestellos-Blanco, S., Zhang, H., Kim, J. M., Shen, Y. xiao & Yang, P. Photosynthetic semiconductor biohybrids for solar-driven biocatalysis. *Nat. Catal.* **3**, 245–255 (2020).

32. Kornienko, N., Zhang, J. Z., Sakimoto, K. K., Yang, P. & Reisner, E. Interfacing nature's catalytic machinery with synthetic materials for semi-artificial photosynthesis. *Nat. Nanotechnol.* **13**, 890–899 (2018).

33. Wang, Y. *et al.* Facile One-Step strategy for highly boosted microbial extracellular electron transfer of the genus *Shewanella*. *ACS Nano* **10**, 6331–6337 (2016).

34. Xiu, Z. M., Zhang, Q. B., Puppala, H. L., Colvin, V. L. & Alvarez, P. J. J. Negligible particle-specific antibacterial activity of silver nanoparticles. *Nano Lett.* **12**, 4271–4275 (2012).

35. Schröder, U., Nießen, J. & Scholz, F. A generation of microbial fuel cells with current outputs boosted by more than one order of magnitude. *Angew. Chemie - Int. Ed.* **42**, 2880–2883 (2003).

36. Ding, C. *et al.* Hybrid bio-organic interfaces with matchable nanoscale topography for durable high extracellular electron transfer activity. *Nanoscale* **6**, 7866–7871 (2014).

37. Xie, X. *et al.* Three-dimensional carbon nanotube-textile anode for high-performance microbial fuel cells. *Nano Lett.* **11**, 291–296 (2011).

38. Mclean, J. S. *et al.* Quantification of electron transfer rates to a solid phase electron acceptor through the stages of biofilm formation from single cells to multicellular communities. *Environ. Sci. Technol.* **44**, 2721–2727 (2010).

39. Gross, B. J. & El-Naggar, M. Y. A combined electrochemical and optical trapping platform for measuring single cell respiration rates at electrode interfaces. *Rev. Sci. Instrum.* **86**, (2015).

40. Shi, L. *et al.* Extracellular electron transfer mechanisms between microorganisms and minerals. *Nat. Rev. Microbiol.* **14**, 651–662 (2016).

41. El-Naggar, M. Y., Gorby, Y. A., Xia, W. & Nealson, K. H. The molecular density of states in bacterial nanowires. *Biophys. J.* **95**, 10–12 (2008).

42. Breuer, M., Rosso, K. M. & Blumberger, J. Electron flow in multiheme bacterial cytochromes is a balancing act between heme electronic interaction and redox potentials. *Proc. Natl. Acad. Sci. U. S. A.* **111**, 611–616 (2014).

43. White, G. F. *et al.* Rapid electron exchange between surface-exposed bacterial cytochromes and Fe(III) minerals. *Proc. Natl. Acad. Sci. U. S. A.* **110**, 6346–6351 (2013).

44. Ross, D. E. *et al.* Characterization of protein-protein interactions involved in iron reduction by *Shewanella oneidensis* MR-1. *Appl. Environ. Microbiol.* **73**, 5797–5808 (2007).

45. McMillan, D. G. G. *et al.* Protein-protein interaction regulates the direction of catalysis and electron transfer in a redox enzyme complex. *J. Am. Chem. Soc.* **135**, 10550–10556 (2013).

46. Marritt, S. J. *et al.* A functional description of CymA, an electron-transfer hub supporting anaerobic respiratory flexibility in *Shewanella*. *Biochem. J.* **444**, 465–474 (2012).

47. Lower, B. H. *et al.* Antibody recognition force microscopy shows that outer membrane cytochromes OmcA and MtrC are expressed on the exterior surface of *Shewanella* oneidensis MR-1. *Appl. Environ. Microbiol.* **75**, 2931–2935 (2009).

48. Shi, L. *et al.* Isolation of a high-affinity functional protein complex between OmcA and MtrC: Two outer membrane decaheme c-type cytochromes of *Shewanella oneidensis* MR-1. *J. Bacteriol.* **188**, 4705–4714 (2006).

49. Brutinel, E. D. & Gralnick, J. A. Preferential utilization of d-Lactate by *Shewanella oneidensis*. *Appl. Environ. Microbiol.* **78**, 8474–8476 (2012).

50. Wodke, J. A. H. *et al.* Dissecting the energy metabolism in *Mycoplasma pneumoniae* through genome-scale metabolic modeling. *Mol. Syst. Biol.* **9**, (2013).

51. Rule, G. S., Pratt, E. A., Chin, C. C. Q., Wold, F. & Ho, C. Overproduction and nucleotide sequence of the respiratory D-lactate dehydrogenase of *Escherichia coli*. *J. Bacteriol.* **161**, 1059–1068 (1985).

52. Pinchuk, G. E. *et al.* Genomic reconstruction of *Shewanella oneidensis* MR-1 metabolism reveals a previously uncharacterized machinery for lactate utilization. *Proc. Natl. Acad. Sci. U. S. A.* **106**, 2874–2879 (2009).

53. LeVan, K. M. & Goldberg, E. Properties of human testis-specific lactate dehydrogenase expressed from *Escherichia coli*. *Biochem. J.* **273**, 587–592 (1991).

54. Zhang, W. *et al.* Highly selective oxidation of ethyl lactate to ethyl pyruvate catalyzed by mesoporous vanadia-titania. *ACS Catal.* **8**, 2365–2374 (2018).

55. Li, J. & Liu, C. Y. Ag/Graphene heterostructures: Synthesis, characterization and optical properties. *Eur. J. Inorg. Chem.* 1244–1248 (2010). doi:10.1002/ejic.200901048

56. Song, R. Bin *et al.* Inkjet-printed porous polyaniline gel as an efficient anode for microbial fuel cells. *J. Mater. Chem. A* **4**, 14555–14559 (2016).

57. Zhao, C. e. *et al.* Hybrid conducting biofilm with built-in bacteria for high-performance microbial fuel cells. *ChemElectroChem* **2**, 654–658 (2015).

58. Mehdinia, A., Ziaei, E. & Jabbari, A. Multi-walled carbon nanotube/SnO_2 nanocomposite: A novel anode material for microbial fuel cells. *Electrochim. Acta* **130**, 512–518 (2014).

59. Ringeisen, B. R. *et al.* High power density from a miniature microbial fuel cell using *Shewanella oneidensis* DSP10. *Environ. Sci. Technol.* **40**, 2629–2634 (2006).

Reduced graphene oxide/copper nanoparticles (rGO/Cu) electrode for high performance microbial fuel cell

4.1 Introduction

As we mentioned in chapter 3, the transmembrane and extracellular electron transfer processes in the exoelectrogenic bacteria generally involve sluggish electron hopping through redox centers in atypical conductors or through multiple redox cycles, which could severely limit the charge transfer efficiency[1–8]. Besides, the *Shewanella* is capable of tolerating heavy metal ions and eventually reduce them as nanoparticles with the extracellular electrons[9,10]. By constructing the metal releasing anode electrode, we realize the enhancement of microbial fuel cell performance with *Shewanella*-Ag hybrids. The resulting *Shewanlla*-Ag hybrids show transmembrane and outermembrane Ag nanoparticles, which can facilitate the extracellular electron transfer. In this chapter, we changed the Ag element to Cu element on the anodic electrode as a follow up of previous work. We expect the Cu will release the Cu^{2+} ion more efficiently with lower oxidation potential and maximize the *Shewanella*-Cu hybrids performance.

4.2 Experimental sections and methods

Synthesis of reduced graphene oxide/Cu nanoparticles (rGO/Cu) composites

Typically, 2 ml of graphene oxide (3 mg/ml) solution is mixed with 30 mg of commercial 50 nm copper nanoparticles and 8 ml of DI water. The whole system is sonicated for over 2h for better mixing. 20 mg of sodium borohydride ($NaBH_4$) is dissolved in 10 ml DI water. Under vigorous stirring, the 10 ml $NaBH_4$ solution is added dropwise, slowly. After 10 min, the entire solution becomes dark black. Stirring is continued overnight at room temperature. The rGO/Cu composite is washed three times with the centrifuge and sonication with the DI water. Finally, the composite is dissolved in 10 ml ethanol for further use.

Fabrication of carbon paper/rGO/Cu nanoparticles anode

The carbon paper (CP) is cut into small pieces, 2 cm^2 (1 cm × 2 cm). 1 ml of the rGO/Cu solution is dropped on carbon paper to form a uniform layer. After that, the sample is dried in air. For carbon paper/rGO anode, the fabrication process and drying are the same.

Bacteria culture

Shewanella oneidensis MR-1 is first inoculated with 20 ml of LB solution. The entire flask together with the LB solution is put in a 30 ℃ shaker for at least 15 h (usually overnight). 200 μL of bacteria colonies are taken out and put in another flask containing 20 ml of fresh LB solution. Before any test, 5 ml of bacteria colonies are taken out, centrifuged and washed 3 times with *Shewanella* medium. The final bacteria solution's OD_{600} is about 1.0.

Half-cell microbial fuel cell experiment

The three electrodes are placed in a three-neck flask. The working electrode is carbon paper or carbon paper/rGO or carbon paper/rGO/Cu. The reference electrode is 1 M KCl Ag/AgCl electrode, and the counter electrode is platinum wire. After adding all the solutions, the entire system is purged with ultra-pure N_2 gas for 30 min to remove dissolved oxygen. In a typical current-time (*I-t*) measurement, a positive potential (200 mV vs. reference electrode) is added on the working electrode and the corresponding electrochemical current is recorded.

Full cell microbial fuel cell experiment

The H-shaped two-chamber MFC is constructed by connecting two 120 ml chambers with a proton exchange membrane (PEM) Nafion 211 separator. The diameter of the chamber channel is 5.5 cm. The cathode is carbon cloth (2 cm × 4 cm) coated with 40% Pt/C with oxygen purging. Before the tests, two sterilization steps are conducted to ensure the device is fully sterilized. Before

constructing the devices, all the plastic chambers are soaked in aqueous detergent solution, and sufficiently rinsed with deionized water. After the devices and membranes are fully constructed, the entire device is immersed into boiling water for 15 min for further sterilization. Before the test, the anodic solution is purged with pure nitrogen gas for 30 min to remove the dissolved oxygen. The anodic chamber is tightly sealed to maintain the anaerobic condition during MFC operation. All MFC experiments are operated at ~30 °C. At MFC steady state, the polarization curves are obtained by varying the external resistor. The output voltage is recorded with a multi-meter. The output current is calculated from Ohm's Law: I=V/R (R is the value of external resistor). The output power is calculated by $P=IV=V^2/R$. For long-standing tests and the EIS tests, the cathode solution is changed to potassium ferricyanide ($K_3[Fe(CN)_6]$, 50 mM) and potassium chloride (KCl, 50 mM).

Scanning electron microscope (SEM) measurement

After MFC testing, the entire anode with the biofilm is fixed by 2.5% glutaraldehyde ($C_5H_8O_2$) solution overnight at 4 °C and chemically dehydrated using gradient concentration ethanol aqueous solution (50, 70, 80, 90, and 95% each one, then 100% twice). The sample was dried in the vacuum chamber and finally sputter-coated gold for further SEM imaging.

Transmission electron microscope (TEM) measurements

After MFC testing, the bacterial solution is taken out, centrifuged and fixed by 2.5% glutaraldehyde ($C_5H_8O_2$) solution overnight at 4 °C and 2% osmium tetroxide (OsO_4) aqueous solution at 4 °C for 4 h. After fixation, the bacteria pellet is chemically dehydrated using gradient concentration of ethanol (50, 70, 80, 90, and 95% once each, then 100% twice) and 100% acetone. The bacteria pellet is finally embedded in the resin (Araldite 502) and polymerized in the oven at

60 ℃ for at least 36 h. Ultrathin sections of 70 nm are cut by an ultratome and deposited on carbon coated copper grids for TEM imaging.

Electrochemical impedance spectroscopy (EIS) measurement

For the R_{ct} of different electrodes without the bacteria, the measurement is conducted in a three-neck flask with bacteria buffer medium and 50 mM $K_3[Fe(CN)_6]$. The three electrodes carbon paper, rGO, and rGO/Ag are set as working electrodes. The Pt wire and Ag/AgCl are set as the counter electrode and the reference electrode, respectively. EIS is measured within the frequency range of 10^5 to 0.5 Hz at the voltage of 0.2 V vs RHE. For the full MFC, the EIS test is conducted after 2 days of MFC setup. The cathode is the potassium ferricyanide ($K_3[Fe(CN)_6]$, 50 mM) and potassium chloride (KCl, 50 mM). The anode is set as the working electrode and the cathode is connected with both the counter and reference electrode.

Confocal laser scanning microscopy (CLSM) measurement

The L7007 live/dead bacterial viability kit is used to evaluate the bacteria viability on the anode. The anode with biofilm after MFC test is rinsed with PBS and stained with SYTO 9 dye and propidium iodide (PI) mix solution. The stained cells are examined using a Leica TCS SP8 II confocal/multiphoton laser scanning microscope (Germany). The alive-dead assay solution is prepared by diluting SYTO 9 dye solution (1.67 mM solution in dimethyl sulfoxide) and propidium iodide (1.67 mM solution in dimethyl sulfoxide) stock solutions in PBS at final concentrations of 30 μM and 30 μM. In living bacteria, the SYTO 9 dye will emit strong green fluorescence. In dead bacteria, the PI will bound to DNA and emit red fluorescence.

Coulombic efficiency (QE) calculations

The Coulombic efficiency is evaluated by the following equations S1-S3. In equation S1, the η is the Coulombic efficiency, C_{output} is the amount of experimental electric quantity in the microbial fuel cell, in Coulombs. In equation S2, t is the total time in seconds. In equation S3, C_{total} is the total theoretical amount of charge (Q, in Coulombs) transferred in the lactate oxidation process. $C_{lactate}$ is the lactate concentration of the bacteria buffer medium. $V_{solution}$ is the total volume of the medium. n: The number of electrons transferred during the oxidation of one molecule of lactate. F is Faraday's constant (96,500 C/mol).

$$\eta = C_{output}/C_{total} \quad \text{(S1)}$$

$$C_{output} = \int (I \cdot t) \quad \text{(S2)}$$

$$C_{total} = C_{lactate} \cdot V_{solution} \cdot n \cdot F \quad \text{(S3)}$$

4.3 Results and discussions

When synthesizing the rGO/Cu electrode, we use the sodium borohydride ($NaBH_4$) as the reducing regent of graphene oxide. Yet for Cu nanoparticles, we chose to directly add the commercial 50 nm Cu nanoparticles at the first beginning with the graphene oxide. As a consequence, the pre-standing Cu nanoparticles are loaded on the rGO layer as the rGO/Cu electrode (**Fig. 4.1d**). Under scanning electron microscopy (SEM, **Fig. 4.1a**) the Cu nanoparticles show numerous white dots compared with bare rGO (**Fig. 4.1a**). With the energy dispersive spectroscopy (EDS, **Fig. 4.1c**), the Cu is proved to be the solitary metal on the electrode.

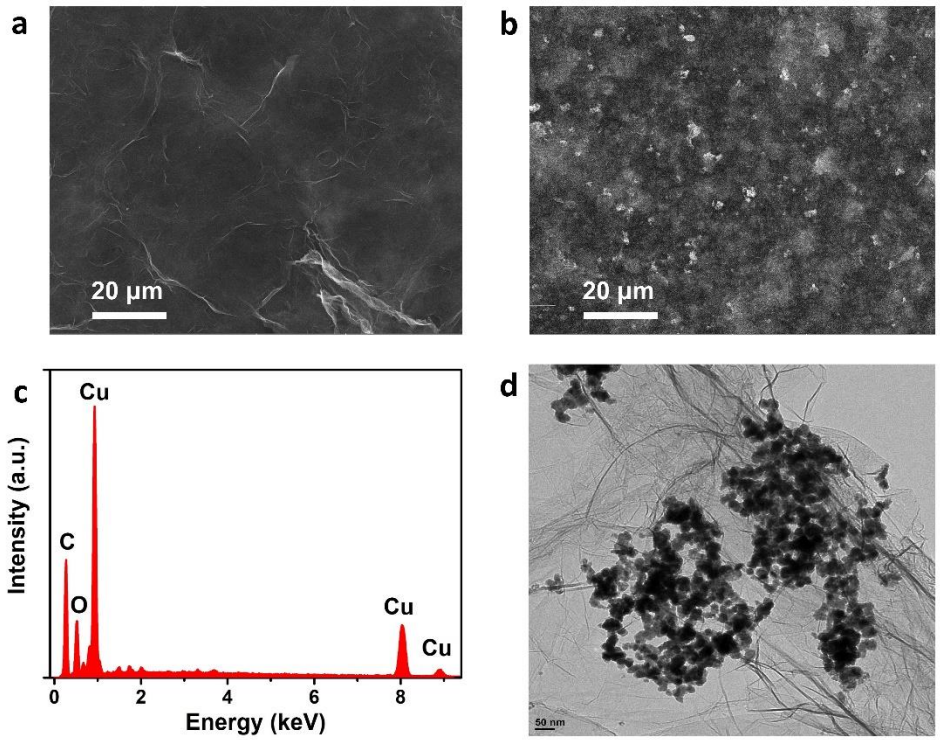

Fig. 4.1 | The physical characterization of rGO/Cu. (a) SEM image of bare rGO. (b) SEM image of rGO/Cu. (c) EDS analysis of rGO/Ag (a.u., arbitrary unit). (d) TEM image of rGO/Cu which shows that the rGO is covered with Cu nanoparticles.

In the microbial fuel cell tests, we used carbon paper as the commercial material benchmark and rGO as the control experiment. After conducting 3 different electrodes in the microbial fuel cell, we first evaluate the scale of the biofilm. For carbon paper, the living cell number under the confocal laser scanning microscopy (CLSM, **Fig. 2a, b**) match well with the SEM pictures (**Fig, 2c, d**), which shows limited number of bacteria. Whereas for rGO, the bacteria number shows increasing trend compared with the carbon paper. For rGO/Cu, the living cell green fluorescence can be also comparable to the SEM images with dense biofilms consist of bar-like bacteria (**Fig, 2i, j, k, l**).

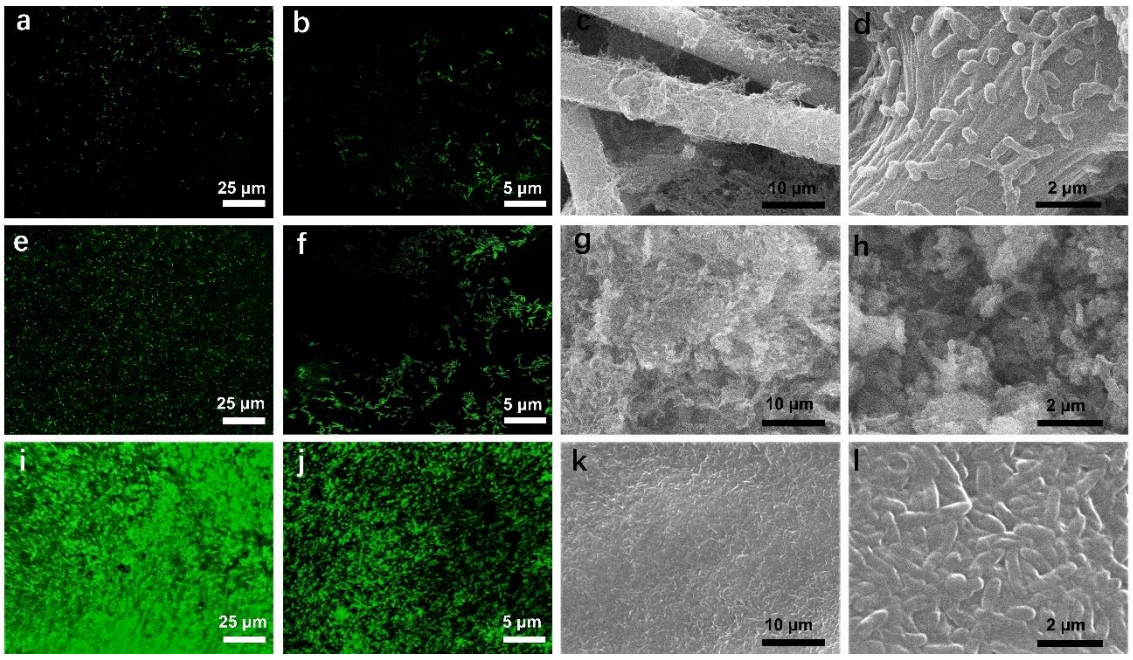

Fig. 4.2 | The characterization of *Shewanella* biofilms on three different anodic electrodes: carbon paper, rGO and rGO/Cu. (a)(b) Confocal laser scanning microscopy (CLSM) images of the *Shewanella* biofilm on the carbon paper. (c)(d) Scanning electron microscope (SEM) images of the biofilm on the carbon paper. (e)(f) CLSM images of biofilm on the rGO. (g)(h) SEM images of biofilm on the rGO. (i)(j) CLSM images of biofilm on the rGO/Cu. (k)(l) SEM images of biofilm on the rGO/Cu.

In the microbial fuel cell tests, we also conducted half cell and full cell for all three electrodes: carbon paper, rGO and rGO/Cu. With no surprise, the carbon paper and the rGO gives relatively low current output compared with the 8.0 A/m^2 from the rGO/Cu (**Fig. 4.3a**). This will further lead us to the full microbial fuel cell tests in the H-shape chambers. Under steady status with the rGO/Cu as the anodic electrode, the maximum power density is 4.6 W/m^2, which is significant higher than those from the carbon paper and rGO (**Fig. 4.3b**). Furthermore, by refreshing the new medium with various amount of lactate, we also test the long-standing capability with 3 electrodes (**Fig. 4.3c**). The power output can recover to the original level with new medium added and the standing time can be even doubled with new medium with doubled concentration of lactate. As a

consequence of the stability test, the Coulombic efficiency (QE) is as high as 72% for the rGO/Cu electrode (**Fig. 4.3d**).

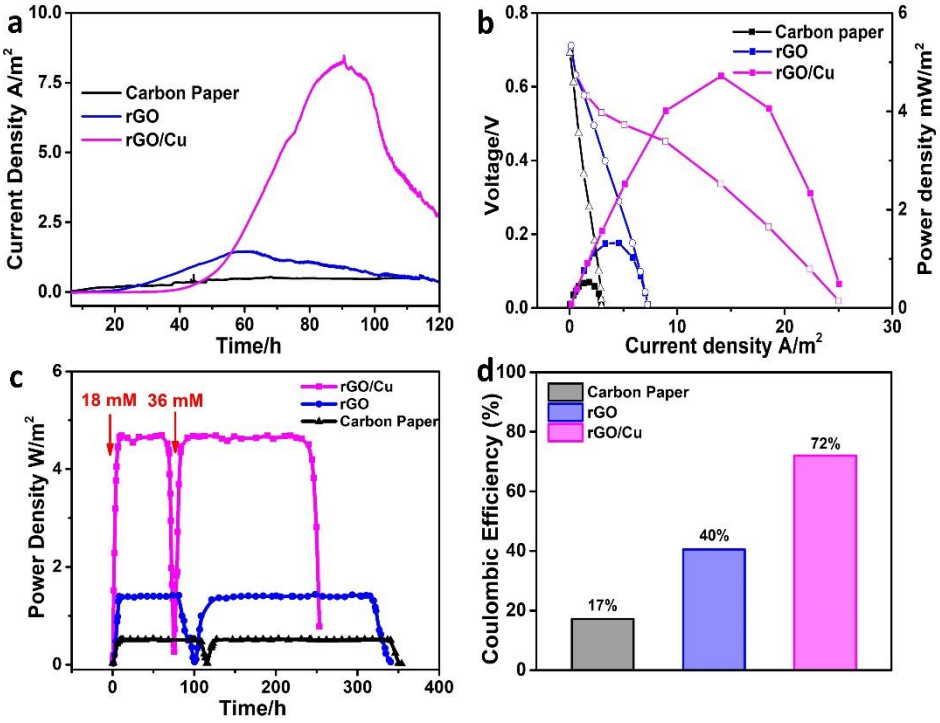

Fig. 4.3 | The performance test of *Shewanella* MFCs with different anodes. (a) Single chamber MFCs with three different anodic materials. (b) MFC I-V curves and power polarization curves of three different anodic materials. (c) MFC power density vs. time curves for long stability and repeated cycling test. (d) The comparison of the Coulombic efficiency (QE) of three different electrodes.

As we mentioned in the chapter 3, the metal releasing electrode will eventually result to the *Shewanella*-metal hybrids after the MFC tests. With the rGO/Cu as the anode, we can see the *Shewanella*-Cu hybrid structure no matter for a full single bacterium or the ultrathin section (**Fig. 4.4**). Besides, for the section of *Shewanella*-Cu hybrid, we can clearly see the Cu nanoparticles in between the inner and outer membrane. This is due to the *Shewanella*'s reducing capability towards Cu ions released by rGO/Cu electrode.

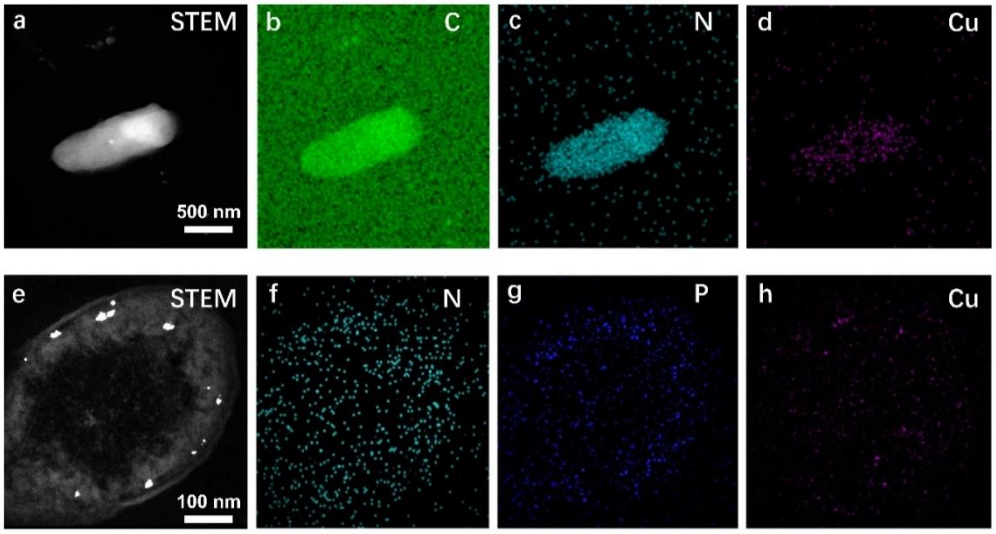

Fig. 4.4 | The EDX element mapping of *Shewanella* and ultrathin sections. (a-d) The *Shewanella* complete cell with Cu nanoparticles. (e-h) The *Shewanella* ultrathin section with Cu nanoparticles.

After estimate the bacteria number on different electrodes with the weight difference, we can also calculate the single bacterium turnover frequency (TOF, **Fig. 4.5**) with the maximum current density obtained from H-shape testing. With Cu nanoparticles embedding into the *Shewanella*, the TOF has raised from ~400,000 s^{-1} to ~670,000 s^{-1}.

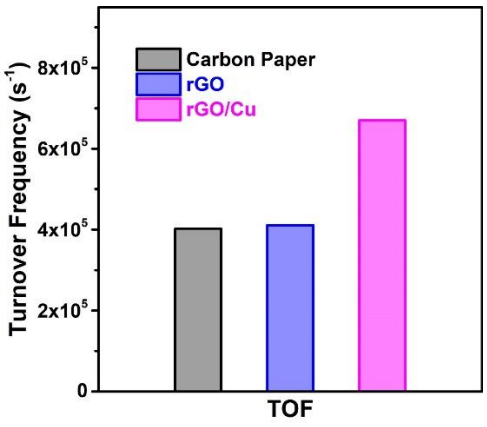

Fig. 4.5 | Single bacterium turnover frequency (TOF) from different electrodes. The TOFs from carbon paper and rGO are comparable, with ~ 400,000 s^{-1}.

To probe the *Shewanella*-Cu hybrids superb extracellular electron transfer ability, we tested the electrochemical impedance spectra (EIS, **Fig. 4.6**) for three different electrodes after one cycle of MFC tests. For three electrodes, the EIS consists of 2 semicircles, which originates from the charge transfer resistance (R_{ct}) from cathode (R_{cath}) and anode reaction ($R_{biofilm}$). The first semicircle, which is from the cathode reduction reaction as almost the same values (~ 7 Ω). For the second semicircle from the biofilm R_{ct}, the 20 Ω $R_{biofilm}$ from the rGO/Cu is far smaller than those from carbon paper and rGO. The much reduced $R_{biofilm}$ further prove the better extracellular electron transfer from the *Shewanella*-Cu hybrids.

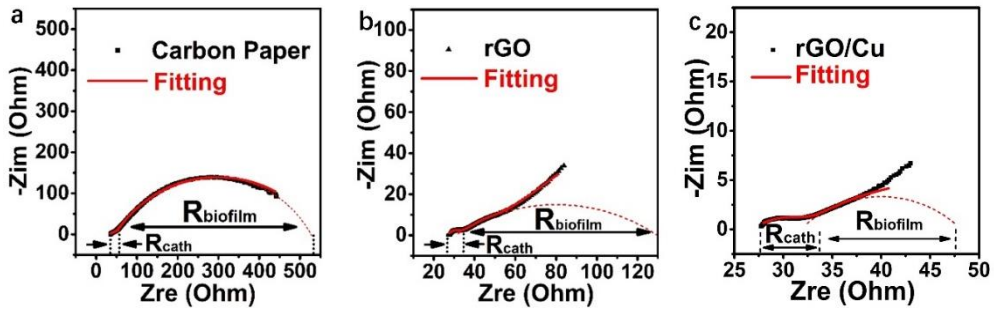

Fig. 4.6 | Electrochemical impedance spectra (EIS) tests of different MFC anodes. The R_{cath} is the charge transfer resistance of ferricyanide cathode reactions. The $R_{biofilm}$ is the charge transfer resistance from the anode bacteria biofilm.

4.4 References

1. Polizzi, N. F., Skourtis, S. S. & Beratan, D. N. Physical constraints on charge transport through bacterial nanowires. *Faraday Discuss.* **155**, 43–61 (2012).

2. Pirbadian, S. & El-Naggar, M. Y. Multistep hopping and extracellular charge transfer in microbial redox chains. *Phys. Chem. Chem. Phys.* **14**, 13802 (2012).

3. Gorby, Y. A. *et al.* Electrically conductive bacterial nanowires produced by *Shewanella oneidensis* strain MR-1 and other microorganisms. *Proc. Natl. Acad. Sci.* **103**, 11358–11363 (2006).

4. Pirbadian, S. *et al. Shewanella oneidensis* MR-1 nanowires are outer membrane and periplasmic extensions of the extracellular electron transport components. *Proc. Natl. Acad. Sci. U. S. A.* **111**, 12883–12888 (2014).

5. El-Naggar, M. Y. *et al.* Electrical transport along bacterial nanowires from *Shewanella oneidensis* MR-1. *Proc. Natl. Acad. Sci. U. S. A.* **107**, 18127–18131 (2010).

6. Ding, M. *et al.* An on-chip electrical transport spectroscopy approach for in situ monitoring electrochemical interfaces. *Nat. Commun.* **6**, 1–9 (2015).

7. McMillan, D. G. G. *et al.* Protein-protein interaction regulates the direction of catalysis and electron transfer in a redox enzyme complex. *J. Am. Chem. Soc.* **135**, 10550–10556 (2013).

8. Shi, L. *et al.* Extracellular electron transfer mechanisms between microorganisms and minerals. *Nat. Rev. Microbiol.* **14**, 651–662 (2016).

9. Jiang, X. *et al.* Nanoparticle facilitated extracellular electron transfer in microbial fuel cells. *Nano Lett.* **14**, 6737–6742 (2014).

10. Wu, X. *et al.* A role for microbial palladium nanoparticles in extracellular electron transfer. *Angew. Chemie - Int. Ed.* **50**, 427–430 (2011).

Chapter 5. Conclusion

Shewanella and other exoelectrogenic bacteria can provide significant chances in bio-energy harvesting and bio-sensing. However, such metabolism behaviors together with the current output features and cell density relationship are still unclear. Besides, exoelectrogenic bacteria based microbial fuel cells are still suffering from low performance output. So that we use *Shewanella*-inorganic hybrids, which include *Shewanella*-nano-device, *Shewanella*-Ag and *Shewanella*-Cu to address these problems.

We first demonstrated a platform with nano-electronic fabrication and measurement to elucidate the origin of the electrical conducting current from *Shewanella oneidensis* MR-1 and 2 other mutants ΔmtrC/ΔomcA and Δbfe. The electrical characteristics of living MR-1, ΔmtrC/ΔomcA and Δbfe were obtained under physiological conditions together with *in situ* real time optical imaging and other on-chip measurement approaches without artificial coloration. Based on those electrochemical current shown on MR-1, ΔmtrC/ΔomcA and Δbfe, the different electron transport pathway was discussed. The methodology reported in this study could explore more fundamental and theoretical studies on EET pathway and also metabolic activities status. Our electrochemistry model provides valuable insights into the elucidation of EET mechanisms by providing experimental supports for the currently proposed “direct electron transfer” mechanism is major factor that unifies the EET mechanism in *Shewanella oneidensis* MR-1.

Taking into a further step, at the level of bacterium modification, we have designed and demonstrated a rGO/Ag anodic electrode for constructing high density *Shewanella* biofilms to enable MFCs with a high current density of 38.5 A/m^2, high power density of 6.63 W/m^2, and Coulombic efficiency of 81%. These values all are the highest reported for MFCs to date. Taking

advantage of the heavy metal ion tolerance of *Shewanella*, the silver ions released by the rGO/Ag electrode can be reduced *in situ* by metabolic electrons to produce trans/outer-membrane Ag nanoparticles, which can greatly boost the transmembrane and extracellular electron transfer to produce higher TOF and higher power output. Our study highlights that engineering *Shewanella*-Ag hybrids with transmembrane metallic nanoparticles provides an effective pathway to break the electron transfer limit in typical natural bacteria and to push the limit of the MFCs. Follow this pathway, we further expand our rGO/Ag electrode to rGO/Cu for new microbial fuel cell electrode.

Based on our result, it is clear that taking single cell level study and modification can break the limit of performance more effectively compared with conducting engineering style boosting. Taking together, by combining the inorganic material such as nano-device chip and nanoparticles with the organism, some insight features of certain bacterium can be well monitored, elucidated and even modified, which leads to the enhanced performance. Such hybrids can well be a vivid interpretation of the art of science and technology.